Notes

Contents

1 Important parameters

Throughout the text we use the geometrized unit system where $c = G = 1$. Here is a list of binary parameters that are valid for any Keplerian orbit.

- Total mass $M = m_1 + m_2$. The secondary-to-primary mass ratio is $q = \frac{m_2}{m_1}$. The symmetric mass ratio is $\eta = \frac{m_1 m_2}{M^2}$. The reduced mass is $\mu = M\eta = M\frac{q}{(1+q)^2}$.

- Distance of nearest approach (pericenter distance) r_p

- Semimajor axis $a = \frac{r_p}{1-e}$ for an elliptic orbit with eccentricity e

- The mean angular frequency (radians per unit time) is from Kepler's third law

$$\omega_{\mathrm{orb}} = \sqrt{\frac{M}{a^3}} = \left(\frac{M(1-e)^3}{r_p^3}\right)^{1/2}. \tag{1}$$

- Orbital period $T = 2\pi\omega_{\mathrm{orb}}^{-1}$

- Vis-viva equation (valid for any Keplerian orbit)

$$v^2 = m_1\left(\frac{2}{r} - \frac{1}{a}\right). \tag{2}$$

1.1 Hyperbolic Keplerian orbits

- Semi-major axis

$$-a = \frac{M}{v^2}$$

- Eccentricity

$$e^2 = 1 + \frac{b^2 v^4}{M^2}$$

- Pericenter distance

$$r_p = -a(e-1) = \frac{M}{v^2}\left[\left(1 + \frac{b^2 v^4}{M^2}\right)^{1/2} - 1\right].$$

Here b is the impact parameter. For small relative velocities v this simplifies to

$$r_p \simeq \frac{b^2 v^2}{2M}\left(1 - \frac{b^2 v^4}{4M^3}\right). \tag{3}$$

1.2 Elliptic Keplerian orbit

- Orbital energy of two orbiting bodies is the sum of their mutual potential energy and their total kinetic energy

$$E = M\eta\left(\frac{v^2}{2} - \frac{M}{r}\right) = -\frac{\eta M^2}{2a}. \tag{4}$$

- The absolute value of the orbital angular momentum is

$$J = \mu\sqrt{Ma(1-e^2)} = \mu\omega_{\text{orb}}a^2\sqrt{1-e^2}. \tag{5}$$

- Eccentricity

$$e^2 = 1 + \frac{2EL^2}{M^2\,\mu^3}. \tag{6}$$

- Escape velocity of a orbiting body at a radius r can be obtained from the vis-viva equation (2) by taking the limit as $a \to \infty$

$$v_{\text{esc}} = \sqrt{\frac{2m_1}{r}}. \tag{7}$$

1.3 Evolution equations of e and a

The evolution equations of the eccentricity and semi-major axis of a bound binary are obtained by differentiating equations (4) and (6). We obtain

$$\frac{d\log a}{dt} = \frac{1}{a}\frac{da}{dt} = -\frac{\dot{E}}{E} + \frac{2\dot{M}}{M} + \frac{\dot{\eta}}{\eta}, \tag{8}$$

and

$$\frac{de}{dt} = \frac{1-e^2}{2e}\left[-\frac{2\dot{L}}{L} - \frac{\dot{E}}{E} + \frac{2\dot{M}}{M} - \frac{3\dot{\mu}}{\mu}\right]. \tag{9}$$

Under the assumption that $\dot{M} = \dot{\mu} = 0$, the last equation can be rewritten as

$$\frac{de}{dt} = \frac{a(1-e^2)}{e\mu M}\left[\dot{E} - \frac{M^{1/2}}{a^{3/2}(1-e^2)^{1/2}}\dot{L}\right]. \tag{10}$$

Thus $\dot{E} < 0$ is a negative contribution to $\dot{e}$ and $\dot{L} < 0$ is a positive contribution to $\dot{e}$.

2 Aspects of gravitational wave emission

In this section we briefly describe the multipole decomposition formalism in linearised general relativity as given by Thorne [1]. Then this formalism is applied to determine in the mass quadrupole approximation the energy loss, angular momentum loss and energy spectrum for binary systems on elliptic and hyperbolic Keplerian orbits.

2.1 Multipole expansion formalism

In the wave zone, gravitational waves can be treated as linearised perturbations propagating on a flat background metric. This background metric can be characterized by a Minkowskiian coordinate system whose origin coincides with the source. In this coordinate frame the transverse and traceless part of the metric perturbation has then the form

$$h_{ij}^{TT} = \frac{1}{r} A_{ij}(t - r, \theta, \phi), \tag{11}$$

where A_{ij} is a traceless and transverse tensor varying in the wave zone rapidly in the radial direction but slowly in the transverse direction. The angular dependence of the radiation field A_{ij} can be decomposed into spherical harmonics. The most suitable set are the pure-spin harmonics with well-defined transversality and helicity properties. Because A_{ij} is traceless and transverse, it contains only the transverse and traceless harmonics $\mathbf{T}^{\mathrm{E2},lm}$ and $\mathbf{T}^{\mathrm{B2},lm}$. The purely longitudinal, purely transversal or mixed longitudinal and transversal components are not encountered in standard general relativity, but need to be included in other metric theories of gravity. For $l = 0$ and $l = 1$ there are no transverse traceless harmonics. Therefore the general form of radiation field has the form

$$h_{ij}^{TT} = \frac{1}{r} \sum_{l=2}^{\infty} \sum_{m=-l}^{l} \left[{}^{(l)}I^{lm}(t - r)\, T_{ij}^{\mathrm{E2},lm} + {}^{(l)}S^{lm}(t - r)\, T_{ij}^{\mathrm{B2},lm} \right]. \tag{12}$$

The expansion coefficients ${}^{(l)}I^{lm}$ and ${}^{(l)}S^{lm}$ are the l-th time derivative of I^{lm} and S^{lm}. The components I^{lm} and S^{lm} are said to be responsible for mass multipole radiation and current multipole radiation respectively. For that reason, the leading order terms I^{2m} are responsible for the mass quadrupole radiation, terms associated with S^{2m} are called current quadrupole contributions, terms arising from I^{3m} are called mass octupole contributions, etc.
The explicit expression of I^{lm} is given by

$$I^{lm} = \frac{16\pi}{(2l + 1)!!} \left(\frac{(l + 1)(l + 2)}{2l(l - 1)} \right)^{1/2} \mathcal{G}_{A_l} \mathcal{Y}_{A_l}^{lm*}, \tag{13}$$

with the mass multipole moments $\mathcal{G}_{A_l}$. The general form of the mass multipole moments $\mathcal{G}_{A_l}$ is given by a sum of several integrals involving the energy-stress tensor and spherical Bessel functions, see equation (5.9a) in [1]. Our calculations will only involve the second mass moments, for which $\mathcal{G}_{A_2}$ in the Newtonian limit becomes equation (18). We also don't need expressions for the current multipole contributions S^{lm} in this work.

The explicit form of the STF tensors $\mathcal{Y}^{2m}_{a_1 a_2}$ is given by

$$\mathcal{Y}^{22}_{a_1 a_2} = \left(\frac{15}{32\pi}\right)^{1/2} \begin{pmatrix} 1 & i & 0 \\ i & -1 & 0 \\ 0 & 0 & 0 \end{pmatrix}_{a_1 a_2}, \tag{14}$$

$$\mathcal{Y}^{21}_{a_1 a_2} = -\left(\frac{15}{32\pi}\right)^{1/2} \begin{pmatrix} 0 & 0 & 1 \\ 0 & 0 & i \\ 1 & i & 0 \end{pmatrix}_{a_1 a_2}, \tag{15}$$

$$\mathcal{Y}^{20}_{a_1 a_2} = \left(\frac{5}{16\pi}\right)^{1/2} \begin{pmatrix} -1 & 0 & 0 \\ 0 & -1 & 0 \\ 0 & 0 & 2 \end{pmatrix}_{a_1 a_2}, \tag{16}$$

together with $\mathcal{Y}^{2-m}_{a_1 a_2} = (-1)^m \left(\mathcal{Y}^{2m}_{a_1 a_2}\right)^*$.

2.1.1 Energy loss

In the multipole formalism the total radiated power is given by

$$P = \frac{dE}{dt} = \frac{1}{32\pi} \sum_{l=2}^{\infty} \sum_{m=-l}^{l} \left\langle |^{(l+1)}I^{lm}|^2 + |^{(l+1)}S^{lm}|^2 \right\rangle. \tag{17}$$

In case of a periodic motion, the brackets denote orbital averaging. In case of a unbound motion, the brackets may be omitted. In what follows, we only consider mass quadrupole radiation. This amounts to considering only contributions arising from I^{2m}. If the source is non-relativistic and has a negligible self-gravity, we can express the second mass moment $\mathcal{G}_{a_1 a_2}$ in terms of the Newtonian mass density ρ

$$\mathcal{G}_{a_1 a_2} = \int d^3x \, \rho \, x_{a_1} x_{a_2}. \tag{18}$$

Then

$$I^{2m} = \frac{16\pi}{5\sqrt{3}} \int d^3x \, \rho \, \mathcal{Y}^{2m*}_{a_1 a_2} \, x_{a_1} x_{a_2} \tag{19}$$

$$\equiv \frac{16\pi}{5\sqrt{3}} \int d^3x \, \rho \, r^2 Y^{2m*}. \tag{20}$$

2.1.2 Angular momentum loss

In the multipole expansion formalism, the change in angular momentum of a system due to gravitational wave emission is given by

$$\frac{dL_j}{dt} = \sum_{l=2}^{\infty} \frac{(l+1)(l+2)}{(l-1)l!(2l+1)!!} \left\langle \epsilon_{jpq} {}^{(l)}\mathcal{G}_{pA_{l-1}} {}^{(l+1)}\mathcal{G}_{qA_{l-1}} \right\rangle \tag{21}$$

$$+ \sum_{l=2}^{\infty} \frac{4l^2(l+2)}{(l-1)(l+1)!(2l+1)!!} \left\langle \epsilon_{jpq} {}^{(l)}\mathcal{S}_{pA_{l-1}} {}^{(l+1)}\mathcal{S}_{qA_{l-1}} \right\rangle. \tag{22}$$

In the mass quadrupole approximation this reduces to

$$\frac{dL_j}{dt} = \frac{2}{5} \left\langle \epsilon_{jpq} {}^{(2)}\mathcal{G}_{pa} {}^{(3)}\mathcal{G}_{qa} \right\rangle. \tag{23}$$

2.2 Application to Keplerian orbit

In this section we calculate, for a Keplerian orbit and for all $e \geqslant 0$, the energy flux, angular momentum flux and energy spectrum resulting from gravitational wave emission in the mass quadrupole approximation.

2.2.1 Energy loss

We choose a coordinate system whose origin coincides with the center of mass of the system and we let the binary lie in the $\theta = \pi/2$-plane. The two masses can then be specified by $(r_1 \cos\phi, r_1 \sin\phi)$ and $(-r_2 \cos\phi, -r_2 \sin\phi)$ with $r_i = \frac{\mu r}{m_i}$. The problem is equivalent to a one body problem of a reduces mass orbiting about the total mass located at the center of mass. Thus we can write

$$I^{2m} = \frac{16\pi}{5\sqrt{3}} \left[m_1 \frac{\mu^2 r^2}{m_1^2} Y^{2m*}\left(\frac{\pi}{2}, \phi\right) + m_2 \frac{\mu^2 r^2}{m_2^2} Y^{2m*}\left(\frac{\pi}{2}, \phi + \pi\right) \right]. \tag{24}$$

The $Y^{2\pm 1*}\left(\frac{\pi}{2}, \phi\right)$ terms vanish, so we get $Y^{2m*}\left(\frac{\pi}{2}, \phi\right) = Y^{2m*}\left(\frac{\pi}{2}, \phi + \pi\right)$. Hence

$$I^{2m} = \frac{16\pi}{5\sqrt{3}} \mu r^2 Y^{2m*}\left(\frac{\pi}{2}, \phi\right). \tag{25}$$

In the quadrupole approximation the power radiated by the system reduces from expression (17) to

$$P = \frac{1}{32\pi} \sum_{m=-2}^{2} |^{(3)}I^{2m}|^2 \tag{26}$$

This expression is also valid for hyperbolic orbits, therefore we refrain at this stage from orbital averaging.
The orbit equations

$$r = \frac{r_p(1+e)}{1 + e\cos\phi}, \tag{27}$$

$$r^2 \frac{d\phi}{dt} = [M_{\text{tot}} r_p (1+e)]^{1/2}. \tag{28}$$

allow the calculation of the time derivatives of I^{2m}. Employing these identities and using the explicit expression of the spherical harmonics Y^{2m*}, the third time derivatives of I^{2m} read

$$^{(3)}I^{20} = \left(\frac{64\pi}{15}\right)^{1/2} \frac{\mu M_{\text{tot}}^{3/2}}{[r_p(1+e)]^{5/2}} \left(1 + e\cos\phi\right)^2 e\sin\phi,$$

$$^{(3)}I^{2-2} = \left(\frac{32\pi}{5}\right)^{1/2} \frac{\mu M_{\text{tot}}^{3/2}}{[r_p(1+e)]^{5/2}} \left(1 + e\cos\phi\right)^2 \left[-e\sin\phi - 4i(1 + e\cos\phi)\right] e^{2i\phi},$$

$$^{(3)}I^{22} = \left(^{(3)}I^{2-2}\right)^*.$$

The radiated power as a function of ϕ along the orbit is then

$$P(\phi) = \frac{8}{15} \frac{\mu^2 M_{\text{tot}}^3}{[r_p(1+e)]^5} \left(1 + e\cos\phi\right)^4 \left[e^2 \sin^2\phi + 12(1 + e\cos\phi)^2\right]. \tag{29}$$

Note that this expression is valid for all values of $e \geq 0$.

Hyperbolic orbit $e \geq 1$: The asymptotes of an hyperbolic orbit are given by $\cos\psi = -1/e$. Thus the total energy released by a binary on an hyperbolic orbit is

$$
\begin{aligned}
E &= \int_{-\psi}^{\psi} P(\phi)\frac{dt}{d\phi}\,d\phi \\
&= \frac{8}{15}\frac{\eta^2 M_{\text{tot}}^{9/2}}{(r(1+e))^{7/2}}\int_{-\psi}^{\psi} d\phi\,(1+e\cos\phi)^2\left[e^2\sin^2\phi + 12(1+e\cos\phi)^2\right] \\
&= \frac{\eta^2 M_{\text{tot}}^{9/2}}{r_p^{7/2}(1+e)^{7/2}}\varrho(e),
\end{aligned}
$$

where

$$
\begin{aligned}
\varrho(e) &= \frac{1}{180}\left[(12(96+292e^2+37e^4)\phi + 48e(96+73e^2)\sin\phi \right. \\
&\qquad \left. + 24e^2(71+12e^2)\sin 2\phi + 368e^3\sin 3\phi + 33e^4\sin 4\phi\right]_{-\psi}^{\psi} \\
&= \frac{64}{5}\left[\left(1+\frac{73}{24}e^2+\frac{37}{96}e^4\right)\cos^{-1}\left(-\frac{1}{e}\right) + \frac{301}{144}(e^2-1)^{1/2}\left(1+\frac{673}{602}e^2\right)\right].
\end{aligned}
$$

For a parabolic orbit, $e=1$, the radiated energy becomes

$$
E = \frac{85\pi}{12\sqrt{2}}\frac{\eta^2 M_{\text{tot}}^{9/2}}{r_p^{7/2}}. \tag{30}
$$

Elliptic orbit $e < 1$: The average of $P(\phi)$ over one orbital period is

$$
\begin{aligned}
\frac{dE}{dt} = P &= \frac{\omega}{2\pi}\int_0^{2\pi} P(\phi)\frac{dt}{d\phi}\,d\phi \\
&= \frac{8}{15}\frac{1}{(1-e^2)^{7/2}}\frac{\mu^2 M_{\text{tot}}^3}{a^5}\int_0^{2\pi}\frac{d\phi}{2\pi}(1+e\cos\phi)^2\left[e^2\sin^2\phi + 12(1+e\cos\phi)^2\right].
\end{aligned}
$$

After performing the integral we arrive at

$$
\frac{dE}{dt} = \frac{32}{5}\frac{\mu^2 M_{\text{tot}}^3}{a^5}\frac{1}{(1-e^2)^{7/2}}\left(1+\frac{73}{24}e^2+\frac{37}{96}e^4\right). \tag{31}
$$

There is a simple way to deduce the energy loss of a parabolic orbit form the energy loss of an elliptic orbit. The energy radiated per orbit is $E = \frac{2\pi}{\Omega}P$. For an hyperbolic orbit, the energy radiated per orbit is the total energy radiated. By analytically continuing the orbital parameters to $e = 1$, we then obtain indeed equation (30). Of course, an extension of the results from $e < 1$ beyond $e = 1$ is not possible.

2.2.2 Angular momentum loss

We now proceed to determine the GW-induced angular momentum loss of a binary on a Keplerian orbit. To this end we choose a coordinate system such that the orbits lies in the (x, y)−plane; then we can set $L = L_z$. Therefore

$$
\frac{dL}{dt} = \frac{2}{5}\left\langle {}^{(2)}\mathcal{G}_{1a}{}^{(3)}\mathcal{G}_{2a} - {}^{(2)}\mathcal{G}_{2a}{}^{(3)}\mathcal{G}_{1a}\right\rangle.
$$

We can integrate the above expression by parts and neglect total derivatives. Even for hyperbolic orbits the total derivatives can be neglected since those terms are the same at $\pm\infty$. Therefore we have, again not writing explicitly the orbital averaging,

$$\frac{dL}{dt} = \frac{4}{5}\,^{(2)}\mathcal{G}_{12}\left(^{(3)}\mathcal{G}_{11} - ^{(3)}\mathcal{G}_{22}\right).$$

The second mass moments in our chosen coordinate frame are given by

$$\mathcal{G}_{a_1 a_2} = \mu r^2 \begin{bmatrix} \cos^2\phi & \cos\phi\sin\phi & 0 \\ \cos\phi\sin\phi & \sin^2\phi & 0 \\ 0 & 0 & 0 \end{bmatrix}_{a_1 a_2}. \tag{32}$$

A calculation of the required derivatives gives

$$^{(2)}\mathcal{G}_{12} = \frac{\mu M}{r_p(1+e)}\sin\phi\,[-4(1+e\cos\phi)^2\cos\phi + 2e(3\cos^2\phi - 1 + 2e\cos^3\phi)],$$

$$^{(3)}\mathcal{G}_{11} = \left(\frac{4\mu^2 M^3}{[r_p(1+e)]^5}\right)^{1/2}(1+e\cos\phi)^2(3e\sin\phi\cos^2\phi + 2\sin(2\phi)),$$

$$^{(3)}\mathcal{G}_{22} = \left(\frac{4\mu^2 M^3}{[r_p(1+e)]^5}\right)^{1/2}(1+e\cos\phi)^2(-e(1+3\cos^2\phi)\sin\phi - 2\sin(2\phi)).$$

The angular momentum emitted as a function of ϕ along the orbit is then

$$\frac{dL}{dt} = \frac{8}{5}\frac{\mu^2 M^{5/2}}{[r_p(1+e)]^{7/2}}(1+e\cos\phi)^2\sin^2\phi \tag{33}$$

$$\times\,[-4(1+e\cos\phi)^2\cos\phi + 2e(3\cos^2\phi - 1 + 2e\cos^3\phi)] \tag{34}$$

$$\times\,[8\cos\phi + 6e\cos^2\phi + e]. \tag{35}$$

Hyperbolic orbit $e \geq 1$:

$$L = \int_{-\psi}^{\psi}\frac{dL}{dt}\frac{dt}{d\phi}\,d\phi \tag{36}$$

$$= \frac{8}{5}\frac{\mu^2 M^2}{[r_p(1+e)]^2}\int_{-\psi}^{\psi}d\phi\,\sin^2(\phi)\,[8\cos\phi + 6e\cos^2\phi + e] \tag{37}$$

$$\times\,[-4(1+e\cos\phi)^2\cos\phi + 2e(3\cos^2\phi - 1 + 2e\cos^3\phi)] \tag{38}$$

$$= \frac{8}{5}\frac{\mu^2 M^2}{[r_p(1+e)]^2}\,\varpi|_{-\psi}^{\psi}, \tag{39}$$

where

$$\varpi = -\frac{7e^2\phi}{2} - 4\phi - 10e\sin\phi + \frac{5}{16}e^2\sin(2\phi) + \frac{5}{2}e\sin(3\phi) + \frac{5}{8}e^2\sin(4\phi)$$

$$+ \sin(4\phi) + \frac{1}{2}e\sin(5\phi) + \frac{1}{16}e^2\sin(6\phi).$$

The evaluation of ϖ between $-\psi = -\cos^{-1}(-1/e)$ and $\psi = \cos^{-1}(-1/e)$ gives

$$\varpi|_{-\psi}^{\psi} = -\left(7e^2 + 8\right)\cos^{-1}\left(-\frac{1}{e}\right) \tag{40}$$

$$+ \frac{(e^2-1)^{1/2}}{e^4}\left(-16 + 8e^2 + 12e^4 + 2e^6 - 21e^8\right). \tag{41}$$

For a parabolic orbit, $e = 1$, the emitted angular momentum becomes

$$L = -6\pi \frac{\mu^2 M^2}{r_p^2}. \tag{42}$$

Elliptic orbit $e < 1$: The angular momentum change averaged over one orbital period is

$$\frac{dL}{dt} = \frac{\omega}{2\pi} \int_0^{2\pi} \frac{dL}{dt} \frac{dt}{d\phi} \, d\phi \tag{43}$$

$$= \frac{8}{10\pi} \frac{\mu^2 M^{5/2}}{a^{3/2} [r_p(1+e)]^2} (1 - e^2)^{3/2} \, \varpi|_0^{2\pi}. \tag{44}$$

The expression $\varpi|_0^{2\pi}$ equals $-(8 + 7e^2)$ and we have

$$\frac{dL}{dt} = -\frac{32}{5} \frac{\mu^2 M^{5/2}}{a^{7/2}} \frac{1}{(1 - e^2)^2} \left(1 + \frac{7}{8} e^2 \right).$$

Analogous to previous subsection, we can perform an analytical continuation of the above result to $e = 1$, thereby again obtaining the parabolic limit (42) of the hyperbolic case. Also, in case of circular motion, the angular momentum flux is directly proportional to the energy flux: $\dot{E} = \omega \dot{L}$.

2.2.3 Frequency spectrum

In this section we compute for all $e \geq 0$ the frequency spectrum of the radiated power. The key ingredient for this is to perform a Fourier decomposition of the binary's second mass moment. The treatise [2] may be used as a reference for the theory of Bessel functions.

Elliptic orbit $e < 1$: We parametrize an elliptic Keplerian orbit in the following form

$$x(\beta) = a(\cos u - e), \tag{45}$$
$$y(\beta) = b \sin u. \tag{46}$$

Here a is the semi-major axis and b is the semi-minor axis of the orbit. The eccentric anomaly u is defined by the Kepler equation

$$u - e \sin u = \Omega t \equiv \beta. \tag{47}$$

The second mass moment has then the form

$$\mathcal{G}_{a_1 a_2} = \mu \begin{bmatrix} a^2 (\cos u - e)^2 & ab(\cos u - e) \sin u & 0 \\ ab(\cos u - e) \sin u & b^2 \sin^2 u & 0 \\ 0 & 0 & 0 \end{bmatrix}_{a_1 a_2} \tag{48}$$

$$= \mu \begin{bmatrix} a^2 (-2e \cos u + \frac{1}{2} \cos(2u) + e^2 + \frac{1}{2}) & ab(-e \sin u + \frac{1}{2} \sin(2u)) & 0 \\ ab(-e \sin u + \frac{1}{2} \sin(2u)) & \frac{b^2}{2} (1 - \cos(2u)) & 0 \\ 0 & 0 & 0 \end{bmatrix}_{a_1 a_2}. \tag{49}$$

9

The emitted power in the mass quadrupole approximation is obtained from the formulae (13) and (26)

$$P = \frac{8\pi}{75} \sum_{m=-2}^{2} \left\langle \left| {}^{(3)}\mathcal{G}_{a_1 a_2} \left(\mathcal{Y}_{a_1 a_2}^{2m} \right)^* \right|^2 \right\rangle \tag{50}$$

$$= \frac{8\pi}{75} \sum_{m=-2}^{2} \frac{1}{2T} \int_{-T}^{T} dt \left| {}^{(3)}\mathcal{G}_{a_1 a_2} \left(\mathcal{Y}_{a_1 a_2}^{2m} \right)^* \right|^2, \tag{51}$$

with the orbital period T. To find the frequency decomposition of the emitted power we can make use of Parseval's identity. This identity asserts equality between the integral of the norm of a periodic function f and the sum of the norm of the function's Fourier coefficients $\mathcal{F}(f)$

$$\frac{1}{2T} \int_{-T}^{T} dt \, |f(t)|^2 = \sum_{n=-\infty}^{\infty} |\mathcal{F}(f)|^2. \tag{52}$$

The effect of the third derivative is to multiply the power spectrum by $(n\Omega)^6$ while at the same time replacing ${}^{(3)}\mathcal{G}_{a_1 a_2}$ by $\mathcal{G}_{a_1 a_2}$. Hence we can write for the radiated power in the n-th harmonic of the orbital angular frequency

$$P_n = 2 \times \frac{8\pi}{75} (n\Omega)^6 \sum_{m=-2}^{2} \left| \mathcal{F} \left(\mathcal{G}_{a_1 a_2} \left(\mathcal{Y}_{a_1 a_2}^{2m} \right)^* \right) \right|^2 \tag{53}$$

$$= \frac{1}{15} (n\Omega)^6 \, \mu^2 \, \Psi, \tag{54}$$

where

$$\Psi = \left| 2a^2 e \, \mathcal{F}(\cos(u)) - \frac{1}{2} \mathcal{F}(\cos(2u)) \left(a^2 - b^2 \right) \right|^2$$

$$+ 3 \left| -2a^2 e \, \mathcal{F}(\cos(u)) + \frac{1}{2} \mathcal{F}(\cos(2u)) \left(a^2 + b^2 \right) \right|^2 \tag{55}$$

$$+ 12 \left| -abe \, \mathcal{F}(\sin(u)) + \frac{ab}{2} \mathcal{F}(\sin(2u)) \right|^2.$$

The factor 2 appearing in equation (53) accounts for the counting of the negative terms in the sum (52). We now proceed with the calculation of the Fourier coefficients of $\sin(mu)$

$$\mathcal{F}(\sin(mu)) = \frac{1}{2\pi} \int_{-\pi}^{\pi} d\beta \, \sin(mu) \, e^{-in\beta}$$

$$= -\frac{1}{2in\pi} \int_{-\pi}^{\pi} du \, \frac{d}{du} \left(e^{-in\beta} \right) \sin(mu)$$

$$= \frac{m}{2in\pi} \int_{-\pi}^{\pi} du \, e^{-in\beta} \, \cos(mu)$$

$$= \frac{m}{2in\pi} \int_{-\pi}^{\pi} du \, \cos(n\beta) \, \cos(mu)$$

$$= \frac{m}{in\pi} \int_{0}^{\pi} du \, \cos(mu) \, \cos(nu - ne \sin u)$$

$$= \frac{m}{2in} \int_{0}^{\pi} \frac{du}{\pi} \left[\cos(u(n+m) - ne \sin u) + \cos(u(n-m) - ne \sin u) \right].$$

By using the following integral representation of the Bessel functions of the first kind

$$J_n(z) = \int_0^\pi \frac{du}{\pi} \cos(nu - z \sin u), \tag{56}$$

we arrive at

$$\mathcal{F}(\sin(mu)) = \frac{m}{2in} \left[J_{n+m}(ne) + J_{n-m}(ne) \right]. \tag{57}$$

A similar calculation gives

$$\mathcal{F}(\cos(mu)) = \frac{m}{2n} \left[-J_{n+m}(ne) + J_{n-m}(ne) \right]. \tag{58}$$

By the use of the recurrence relations

$$J_{n-1}(z) + J_{n+1}(z) = \frac{2n}{z} J_n(z), \tag{59}$$

$$J_{n-1}(z) - J_{n+1}(z) = 2J_n'(z), \tag{60}$$

we can express the Fourier coefficients entirely in terms of J_n and its derivative. We obtain

$$\mathcal{F}(\sin(u)) = \frac{1}{ine} J_n(ne), \tag{61}$$

$$\mathcal{F}(\cos(u)) = \frac{1}{n} J_n'(ne), \tag{62}$$

$$\mathcal{F}(\sin(2u)) = \frac{1}{in} \left[\left(\frac{4}{e^2} - 2 \right) J_n(ne) - \frac{4}{ne} J_n'(ne) \right], \tag{63}$$

$$\mathcal{F}(\cos(2u)) = \frac{1}{n} \left[\frac{4}{e} J_n'(ne) - \frac{4}{ne^2} J_n(ne) \right]. \tag{64}$$

We can insert the above Fourier coefficients into expression (55) and we obtain after rearranging

$$
\begin{aligned}
P_n = {} & \frac{16}{15} (n\Omega)^6 \mu^2 \\
& \times \Bigg\{ J_n^2(ne) \left[(a^4 + b^4) \frac{1}{n^4 e^4} + a^2 b^2 \left(\frac{1}{n^4 e^4} + \frac{3}{n^2 e^4} - \frac{6}{n^2 e^2} + \frac{3}{n^2} \right) \right] + \\
& \quad J_n'^2(ne) \left[a^4 \left(\frac{e^2}{n^2} + \frac{1}{n^2 e^2} - \frac{1}{n^2} \right) + b^4 \frac{1}{n^2 e^2} + a^2 b^2 \left(\frac{1}{n^2 e^2} + \frac{3}{n^4 e^2} \right) \right] + \\
& \quad J_n(ne) J_n'(ne) \left[a^4 \left(\frac{2}{n^3 e} - \frac{2}{n^3 e^3} \right) - b^4 \frac{2}{n^3 e^3} + a^2 b^2 \left(\frac{7}{n^3 e} - \frac{8}{n^3 e^3} \right) \right] \Bigg\}.
\end{aligned} \tag{65}
$$

Parseval's identity allowed us at one stroke to implement the orbital averaging and to decompose the emitted radiation into its harmonics. In appendix (6.1) there is a slightly less straightforward derivation of the frequency spectrum P_n that goes around Parseval's identity.

Hyperbolic orbit $e \geq 1$: The calculation of the frequency spectrum of an hyperbolic orbits follows the same lines as the calculation of the elliptic one. In fact, with a little thought one can deduce from equation (65) most of the structure of the hyperbolic frequency spectrum. However, we will first close our eyes to this fact and present a detailed outline of the calculation. In the end we argue how the result could have been inferred from the elliptic case.

We parametrize the coordinates on an hyperbolic orbit as

$$x = a(e - \cosh u), \tag{66}$$

$$y = b \sinh u, \tag{67}$$

where u satisfies the hyperbolic Kepler equation

$$e \sinh(u) - u = \Omega t. \tag{68}$$

The second mass moment (18) has thus the form

$$\mathcal{G}_{a_1 a_2} = \mu \begin{bmatrix} a^2(e - \cosh u)^2 & ab(e - \cosh u)\sinh u & 0 \\ ab(e - \cosh u)\sinh u & b^2 \sinh^2 u & 0 \\ 0 & 0 & 0 \end{bmatrix}_{a_1 a_2} \tag{69}$$

$$= \mu \begin{bmatrix} a^2(e^2 - 2e\cosh u + \frac{1}{2}\cosh(2u) + \frac{1}{2}) & ab(e\sinh u - \frac{1}{2}\sinh(2u)) & 0 \\ ab(e\sinh u - \frac{1}{2}\sinh(2u)) & \frac{b^2}{2}\cosh(2u) - \frac{b^2}{2} & 0 \\ 0 & 0 & 0 \end{bmatrix}_{a_1 a_2} . \tag{70}$$

We can decompose the total radiated energy in the frequency domain as follows

$$E = \frac{8\pi}{75} \int_{-\infty}^{\infty} dt \sum_{m=-2}^{2} \left| {}^{(3)}\mathcal{G}_{a_1 a_2} \left(\mathcal{Y}_{a_1 a_2}^{2m}\right)^* \right|^2 \tag{71}$$

$$= \frac{1}{2\pi} \frac{8\pi}{75} \int_{-\infty}^{\infty} d\omega \sum_{m=-2}^{2} \left| \widehat{\left[{}^{(3)}\mathcal{G}_{a_1 a_2} \left(\mathcal{Y}_{a_1 a_2}^{2m}\right)^* \right]} \right|^2 \tag{72}$$

$$\equiv \frac{1}{2\pi} \int_{-\infty}^{\infty} d\omega \, P(\omega) = \frac{1}{\pi} \int_{0}^{\infty} d\omega \, P(\omega), \tag{73}$$

where the second equality follows from Plancherel's theorem and the hat represents the Fourier transform. We can take the derivative

$$P(\omega) = \frac{8\pi}{75} \omega^6 \sum_{m=-2}^{2} \left| \left(\mathcal{Y}_{a_1 a_2}^{2m}\right)^* \widehat{\mathcal{G}_{a_1 a_2}} \right|^2, \tag{74}$$

and it remains to calculate the Fourier transform of $\mathcal{G}_{a_1 a_2}$, that is

$$\widehat{\mathcal{G}_{a_1 a_2}} = \int_{-\infty}^{\infty} du \, \frac{dt(u)}{du} \, e^{-i\omega t(u)} \, \mathcal{G}_{a_1 a_2}$$

$$= -\frac{1}{i\omega} \int_{-\infty}^{\infty} du \, \frac{d}{du} \left(e^{-i\omega t(u)} \right) \mathcal{G}_{a_1 a_2}.$$

We will outline the remaining calculation for the $\sinh(nu)$ terms

$$\widehat{\sinh(nu)} = -\frac{1}{i\omega} \int_{-\infty}^{\infty} du \, \frac{d}{du} \left(e^{-i\omega t(u)} \right) \sinh(nu)$$

$$= \frac{n}{i\omega} \int_{-\infty}^{\infty} du \, e^{-i\omega t(u)} \cosh(nu)$$

$$= \frac{n}{2i\omega} \int_{-\infty}^{\infty} du \, e^{-i\frac{\omega}{\Omega}(e \sinh u - u)} \left(e^{nu} + e^{-nu} \right)$$

$$= \frac{n}{2i\omega} \int_{-\infty}^{\infty} du \left(e^{-i\frac{\omega}{\Omega} e \sinh u + (i\frac{\omega}{\Omega} + n)u} + e^{-i\frac{\omega}{\Omega} e \sinh u + (i\frac{\omega}{\Omega} - n)u} \right).$$

This result can be expressed in terms of modified Bessel functions of the second kind $K_\nu(x)$. One possible integral representation of $K_\nu(x)$ has the form

$$K_\nu(x) = \frac{1}{2} e^{\frac{1}{2}\nu\pi i} \int_{-\infty}^{\infty} dt \, e^{-ix \sinh t + \nu t}. \tag{75}$$

With this we can write

$$\widehat{\sinh(nu)} = \frac{n}{i\omega} e^{\frac{1}{2}\frac{\omega}{\Omega}\pi} e^{-\frac{1}{2}n\pi i} \left[K_{i\frac{\omega}{\Omega}+n}\left(\frac{\omega}{\Omega}e\right) + e^{i\pi n} K_{i\frac{\omega}{\Omega}-n}\left(\frac{\omega}{\Omega}e\right) \right]. \tag{76}$$

For the relevant terms for $\widehat{\mathcal{G}_{a_1 a_2}}$ we get

$$\widehat{\sinh(u)} = -\frac{1}{\omega} e^{\frac{1}{2}\frac{\omega}{\Omega}\pi} \left[K_{i\frac{\omega}{\Omega}+1}\left(\frac{\omega}{\Omega}e\right) - K_{i\frac{\omega}{\Omega}-1}\left(\frac{\omega}{\Omega}e\right) \right], \tag{77}$$

$$\widehat{\sinh(2u)} = -\frac{2}{i\omega} e^{\frac{1}{2}\frac{\omega}{\Omega}\pi} \left[K_{i\frac{\omega}{\Omega}+2}\left(\frac{\omega}{\Omega}e\right) + K_{i\frac{\omega}{\Omega}-2}\left(\frac{\omega}{\Omega}e\right) \right]. \tag{78}$$

The calculation of $\widehat{\cosh(nu)}$ proceeds the same way and one finds

$$\widehat{\cosh(nu)} = \frac{n}{i\omega} e^{\frac{1}{2}\frac{\omega}{\Omega}\pi} e^{-\frac{1}{2}n\pi i} \left[K_{i\frac{\omega}{\Omega}+n}\left(\frac{\omega}{\Omega}e\right) - e^{i\pi n} K_{i\frac{\omega}{\Omega}-n}\left(\frac{\omega}{\Omega}e\right) \right], \tag{79}$$

so that we have

$$\widehat{\cosh(u)} = -\frac{1}{\omega} e^{\frac{1}{2}\frac{\omega}{\Omega}\pi} \left[K_{i\frac{\omega}{\Omega}+1}\left(\frac{\omega}{\Omega}e\right) + K_{i\frac{\omega}{\Omega}-1}\left(\frac{\omega}{\Omega}e\right) \right], \tag{80}$$

$$\widehat{\cosh(2u)} = -\frac{2}{i\omega} e^{\frac{1}{2}\frac{\omega}{\Omega}\pi} \left[K_{i\frac{\omega}{\Omega}+2}\left(\frac{\omega}{\Omega}e\right) - K_{i\frac{\omega}{\Omega}-2}\left(\frac{\omega}{\Omega}e\right) \right]. \tag{81}$$

We can now use the recurrence relations

$$K_\nu(x) = -\frac{x}{2\nu} [K_{\nu-1}(x) - K_{\nu+1}(x)], \tag{82}$$

$$K_\nu'(x) = -\frac{1}{2} [K_{\nu-1}(x) + K_{\nu+1}(x)], \tag{83}$$

to derive the following identities

$$K_{\nu+2}(x) + K_{\nu-2}(x) = \left(\frac{4\nu^2}{x^2} + 2 \right) K_\nu(x) - \frac{4}{x} K_\nu'(x), \tag{84}$$

$$K_{\nu+2}(x) - K_{\nu-2}(x) = -\frac{4\nu}{x} K_\nu'(x) + \frac{4\nu}{x^2} K_\nu(x). \tag{85}$$

13

Combining the above we arrive at

$$\widehat{\sinh(u)} = -\frac{2i}{\omega e} \, e^{\frac{1}{2}\frac{\omega}{\Omega}\pi} \, K_{i\frac{\omega}{\Omega}}\left(\frac{\omega}{\Omega}e\right), \tag{86}$$

$$\widehat{\sinh(2u)} = -\frac{2}{i\omega} \, e^{\frac{1}{2}\frac{\omega}{\Omega}\pi} \left[\left(\frac{-4}{e^2}+2\right) K_{i\frac{\omega}{\Omega}}\left(\frac{\omega}{\Omega}e\right) - \frac{4}{\frac{\omega}{\Omega}e} K'_{i\frac{\omega}{\Omega}}\left(\frac{\omega}{\Omega}e\right)\right], \tag{87}$$

$$\widehat{\cosh(u)} = \frac{2}{\omega} \, e^{\frac{1}{2}\frac{\omega}{\Omega}\pi} \, K'_{i\frac{\omega}{\Omega}}\left(\frac{\omega}{\Omega}e\right), \tag{88}$$

$$\widehat{\cosh(2u)} = \frac{8}{e\omega} \, e^{\frac{1}{2}\frac{\omega}{\Omega}\pi} \left[K'_{i\frac{\omega}{\Omega}}\left(\frac{\omega}{\Omega}e\right) - \frac{1}{\frac{\omega}{\Omega}e} K_{i\frac{\omega}{\Omega}}\left(\frac{\omega}{\Omega}e\right)\right]. \tag{89}$$

From equation (74) for the radiated power in the frequency domain we find

$$P(\omega) = \frac{1}{30} \, \omega^6 \, \mu^2 \, \Pi, \tag{90}$$

where

$$\Pi = \left| 2a^2 e \, \widehat{\cosh(u)} - \frac{1}{2}\widehat{\cosh(2u)} \left(a^2+b^2\right) \right|^2$$
$$+ 3 \left| -2a^2 e \, \widehat{\cosh(u)} + \frac{1}{2}\widehat{\cosh(2u)} \left(a^2-b^2\right) \right|^2 \tag{91}$$
$$+ 12 \left| abe \, \widehat{\sinh(u)} - \frac{ab}{2}\widehat{\sinh(2u)} \right|^2.$$

The solutions of the elliptic and hyperbolic frequency spectrum are related by a sort of analytic continuation. Indeed, we can deduce the hyperbolic solution by modifying the calculation of the elliptic case as follows:

1. The hyperbolic Kepler equation (68) is obtained from the elliptic one (equation (47)) by setting $u \mapsto iu$ and $\Omega \mapsto -i\Omega$. Hence $\sin(nu) \mapsto i\sinh(nu)$ and $\cos(nu) \mapsto i\cosh(nu)$.

2. The Fourier coefficients become Fourier transforms and $n\Omega \mapsto \omega$.

3. The energy radiated per orbit into the n-th harmonic, *i.e.* $E(n) = \frac{2\pi}{\Omega}P(n)$, becomes the total energy radiated into the n-th harmonic.

3 Formation of binaries through gravitational wave capture

When two black holes on a parabolic trajectory have a near encounter, they may release sufficiently energy through gravitational waves to form a bound binary. The here adopted simplified picture assumes a sudden energy release at the orbit's pericenter, which then induces a sudden transition from an hyperbolic to an elliptic orbit. To understand the orbit transition more deeply, more work is needed since it is likely that non-linear effects of general relativity have to be considered.

In the center of mass system, the initial energy of two non-interacting black holes is $E_{\text{ini}} = \frac{\mu v^2}{2}$, while the angular momentum of the system reads $L_{\text{ini}} = \mu v b$. Conservation of energy and angular momentum of the system before and after the encounter gives the equations

$$E_{\text{fin}} = \frac{\mu v^2}{2} - \frac{85\pi}{12\sqrt{2}} \frac{\eta^2 M^{9/2}}{r_p^{7/2}}, \tag{92}$$

$$L_{\text{fin}} = \mu v b - 6\pi \frac{\mu^2 M^2}{r_p^2}, \tag{93}$$

where the rightmost terms are the released energy though gravitational waves during a parabolic encounter and the amount of angular momentum lost during a parabolic encounter respectively. For there to form a bound binary system, the energy after the encounter E_{fin} must be negative. Accordingly, the maximal impact parameter of two colliding BHs with relative velocity v to form a binary is

$$b_{\text{max}} = M \left(\frac{340\pi}{3}\right)^{1/7} \left(\frac{\eta}{v^9}\right)^{1/7}, \tag{94}$$

where we used equation (3), the pericenter distance r_p expanded to first order in the relative velocity v. The orbital semi-major axis after the encounter is

$$a_0 = \frac{\mu M}{2|E_{\text{fin}}|}, \tag{95}$$

while the orbital eccentricity after the encounter reads

$$e_0^2 - 1 = \frac{2E_{\text{fin}} L_{\text{fin}}^2}{M^2 \mu^3} = \frac{2E_{\text{fin}} v^2 b^2}{M^2 \mu}. \tag{96}$$

In the last equation we neglected the angular momentum loss due to gravitational wave emission as it is commonly done subsequent to the work of O'Leary *et al.* [3], which found that for typical encounters $L_{\text{fin}} \approx \mu v b$. Substituting b_{max} into equation (3) the corresponding maximum pericenter distance reads

$$r_{p,\text{max}} = 2^{-3/7} M_{\text{tot}} \left(\frac{85\pi}{3}\right)^{2/7} v^2 \left(\frac{t}{v^9}\right)^{2/7} \left[1 - 2^{-10/7} \left(\frac{85\pi}{3}\right)^{2/7} v^4 \left(\frac{t}{v^9}\right)^{2/7}\right]. \tag{97}$$

4 Dynamics affecting the binary's orbital evolution

4.1 GW-driven inspiral of binary

The orbital parameters of a binary system are affected due to the release of gravitational waves. We derive the evolution equations of the semi-major axis and the eccentricity of an elliptical Keplerian orbit.

Substituting the energy loss equation (31) into the evolution equation (8) one finds the gravitational wave driven evolution of the semi-major axis

$$\frac{da}{dt} = -\frac{64}{5}\frac{\mu M_{\text{tot}}^2}{a^3}\frac{1}{(1-e^2)^{7/2}}\left(1 + \frac{73}{24}e^2 + \frac{37}{96}e^4\right). \tag{98}$$

Substituting both (31) and (45) into the evolution equation (10) one finds the gravitational wave driven evolution of the orbital eccentricity

$$\frac{de}{dt} = -\frac{304}{15}\frac{\mu M_{\text{tot}}^2}{a^4}\frac{e}{(1-e^2)^{5/2}}\left(1 + \frac{121}{304}e^2\right). \tag{99}$$

Combining equations (98) and (99) gives

$$\frac{da}{de} = \frac{12}{19}a\frac{1 + (73/24)e^2 + (37/96)e^4}{e(1-e^2)\left(1 + e^2\frac{121}{304}\right)}. \tag{100}$$

The solution of the differential equation (100) is

$$a(e) = c_0\frac{e^{12/19}}{1-e^2}\left(1 + \frac{121}{304}e^2\right)^{870/2299}, \tag{101}$$

where c_0 depends on the initial semi-major axis a_0 and the initial orbital eccentricity e_0. By requiring $a(e_0) = a_0$, we can set

$$c_0 = a_0\left(1 - e_0^2\right)e_0^{-12/19}\left(1 + \frac{121}{304}e_0^2\right)^{-\frac{870}{2299}}.$$

From the orbit equation (1) we can determine the orbital frequency as a function of the eccentricity

$$\frac{\omega}{\omega_0} = \left[\left(\frac{e}{e_0}\right)^{\frac{12}{19}}\frac{1-e_0^2}{1-e^2}\left(\frac{1+\frac{121}{304}e^2}{1+\frac{121}{304}e_0^2}\right)^{\frac{870}{2299}}\right]^{-3/2}, \tag{102}$$

with the initial orbital frequency $\omega_0 = \sqrt{\frac{M}{a_0^3}}$.

To find the time to coalescence τ we can integrate the inverse to equation (99) by requiring that $e(\tau) = 0$, for at coalescence the eccentricity goes to zero. The time to merger is thus given by the integral

$$\tau = \frac{15}{304}\frac{1}{\mu M_{\text{tot}}^2}\int_0^{e_0} de\, a^4\frac{(1-e^2)^{5/2}}{e}\left(1 + \frac{121}{304}e^2\right)^{-1}. \tag{103}$$

We now simplify this expression for an initial orbit whose eccentricity is close to unity. We write the last equation using equation (101) and note that the integral is dominated by e near 1, thus giving

$$\tau = a_0^4 \frac{15}{304} \frac{1}{\mu M_{\text{tot}}^2} \left(1 - e_0^2\right)^4 \int_0^{e_0} de \, \frac{(1 - e^2)^{5/2}}{(1 - e^2)^4} \left(1 + \frac{121}{304}\right)^{-1} \tag{104}$$

$$= a_0^4 \frac{15}{425} \frac{1}{\mu M_{\text{tot}}^2} \left(1 - e_0^2\right)^4 \int_0^{e_0} de \, (1 - e^2)^{-3/2} \tag{105}$$

$$\approx a_0^4 \frac{15}{425} \frac{1}{\mu M_{\text{tot}}^2} \frac{\left(1 - e_0^2\right)^4}{(1 - e_0^2)^{1/2}} = a_0^4 \frac{3}{85} \frac{1}{\mu M_{\text{tot}}^2} \left(1 - e_0^2\right)^{7/2}. \tag{106}$$

As initial semi-major axis a_0 and initial eccentricity e_0 for the bound binary we use the expressions (4) and (6). The time to merger is thus

$$\tau = \left(\frac{\eta M_{\text{tot}}^2}{2E_{\text{fin}}}\right)^4 \frac{3}{85} \frac{1}{\mu M_{\text{tot}}^2} \left(\frac{2E_{\text{fin}} v^2 b^2}{M_{\text{tot}}^2 \mu}\right)^{7/2} \tag{107}$$

$$= \frac{3\sqrt{2}}{170} \frac{1}{E_{\text{fin}}^{1/2} M_{\text{tot}}} \frac{\eta^4}{\mu^{9/2}} v^7 b^7. \tag{108}$$

As the merger time depends on v to the seventh power, we can ignore the contribution of the kinetic part of the final energy E_{fin} and thus use for E_{fin} the expression (30). In this approximation, and upon expressing r_p in δE with its parametrized form (3), the merger time reads

$$\tau = \frac{3}{170} \sqrt{\frac{3}{85\pi}} \frac{(bv)^{21/2}}{\eta^{3/2} M_{\text{tot}}^{19/2}}. \tag{109}$$

4.2 Disk - BBH dynamics

We assume the binary to be embedded in a gaseous disk. The interaction between the binary system and the gaseous disk in which it is embedded is complicated and several mechanisms are at play. Examining the dynamics without resorting to hydrodynamical simulations seems unfruitful.

At some point, the tidal torques exerted by the binary onto the disc are sufficiently high to repel gas away from the binary, thus clearing a cavity around the binary. Furthermore, the binary may then be surrounded by a circumbinary disc which affects the orbital evolution of the central binary. The disc-binary interaction drives the binary ultimately into the phase of GWs-driven inspiral, where loss of orbital energy and angular momentum is due to the emission of gravitational waves.

4.2.1 (Simplified) model of AGN

The equation for hydrostatic equilibrium in the vertical direction for a geometrically thin disk in a central gravitational potential is

$$\frac{dp}{dz} = -\rho \frac{Mz}{r^3}, \tag{110}$$

where $p(r, z)$ and $\rho(r, z)$ are the pressure and mass density at radius r and height z. We assume the disk to be isothermal in the vertical direction; this

yields $c_s^2 = \frac{p}{\rho}$, where c_s is the sound speed (independent of z). Hence we obtain for the mass density

$$\rho = \rho_0 e^{-\frac{z^2}{2h^2}}, \tag{111}$$

with the density at the equatorial plane ρ_0 and with the disk scale height

$$h = \frac{c_s r^{3/2}}{M^{1/2}} = \frac{c_s}{\Omega}. \tag{112}$$

The total mass enclosed within a radius r is denoted by $M(r)$ and is related to the surface density $\Sigma(r)$ through $\frac{dM(r)}{dr} = 2\pi r \Sigma(r)$. In the AGN model outlined in Thompson *et al.* [4], the disk mass $M(r)$ is set to $2\sigma^2 r$, where σ stands for the velocity dispersion of the gas. The associated surface density is then

$$\Sigma(r) = \frac{\sigma^2}{\pi r}. \tag{113}$$

Furthermore, the following relations are imposed to the disk data

$$\frac{f_g}{2^{3/2}} = \frac{h}{r} = \frac{1}{\sqrt{2}} \frac{c_s}{\sigma}, \tag{114}$$

where $f_g = \frac{\Sigma}{\Sigma_g}$ is the total surface density Σ divided by the gas surface density Σ_g. The last relation is a stability criterion.

4.2.2 A little on accretion disks

Viscous Torque in the Disc Because the angular velocity of the accretion disk varies with radius, a viscous torque is acting on the gas. This torque represents the amount of angular momentum crossing the disk circumference at radius r per unit time due to the action of viscosity. The shear stress is $\tau = \rho(r)\nu r \frac{d\Omega}{dr}$, where ν is the dynamical viscosity and $\rho(r)$ the mass density. This leads to a viscous torque between two neighbouring disk annuli at radius r

$$T_{\text{visc}} = 2\pi r \int dz\, r\tau = 2\pi\nu\Sigma(r)r^3 \frac{d\Omega}{dr}, \tag{115}$$

where $\Sigma(r) = \int dz\, \rho(r)$ is the surface density of the disk. By employing the Keplerian orbital frequency it follows that the torque is

$$T_{\text{visc}} = -3\pi\nu\Sigma(r)r^2\Omega(r). \tag{116}$$

One may employ the $\alpha-$disk prescription to parametrize the dynamical viscosity in the case for a thin accretion disk as $\nu = \alpha c_s^2(r)\Omega(r)^{-1}$, where $c_s(r)$ is the local gas sound speed and $0 \leq \alpha \leq 1$ is a dimensionless constant ($\alpha = 0$ corresponds to no accretion). Substituting this expression for ν into the formula for T_{visc} gives

$$T_{\text{visc}} = -3\pi\alpha c_s^2(r)\Sigma(r)r^2. \tag{117}$$

Note that this torque is negative, resulting in an outward transfer of angular momentum.

Continuity equation for accretion disks Suppose that a gaseous disk has surface density $\Sigma(r)$ and radial velocity $v_\phi = r\Omega(r)) = \frac{\dot{M}}{r}$. The structure and the evolution of gaseous disks can be deduced from the continuity equation

$$2\pi r \frac{\partial \Sigma}{\partial t} = \frac{\partial \dot{M}}{\partial r}, \tag{118}$$

and from angular momentum conservation

$$\frac{\partial(\Omega r^2)}{\partial r}\dot{M} = \frac{\partial}{\partial r}(T_{\text{visc}}). \tag{119}$$

Combining equations (118) and (119) gives an evolution equation for the surface density Σ,

$$\frac{\partial \Sigma}{\partial t} = \frac{1}{2\pi r}\frac{\partial}{\partial r}\left[\left(\frac{\partial(\Omega r^2)}{\partial r}\right)^{-1}\frac{\partial(T_{\text{visc}})}{\partial r}\right]. \tag{120}$$

We can incorporate external effects interacting with the disk into the viscous evolution equation of the disk. If the disk experiences an external torque per unit mass $\tilde{T}_{\text{ext}}$, we modify the surface density evolution in the following form

$$\frac{\partial \Sigma}{\partial t} = \frac{1}{2\pi r}\frac{\partial}{\partial r}\left[\left(\frac{\partial(\Omega r^2)}{\partial r}\right)^{-1}\frac{\partial(T_{\text{visc}})}{\partial r} + \frac{4\pi\Sigma\tilde{T}_{\text{ext}}}{\Omega}\right] \tag{121}$$

$$= \frac{1}{2\pi r}\frac{\partial}{\partial r}\left[\left(\frac{\partial(\Omega r^2)}{\partial r}\right)^{-1}\frac{\partial(T_{\text{visc}} + T_{\text{ext}})}{\partial r}\right], \tag{122}$$

defining $\frac{\partial T_{\text{ext}}}{\partial r} = 8\pi\Sigma\tilde{T}_{\text{ext}}r$.

4.2.3   Orbital evolution

Numerical simulations suggest the presence of a depleted cavity inside of which the binary resides. The gas orbiting around this cavity is referred to as the circumbinary disk (CBD). The evolution of the semi-major axis and of the orbital eccentricity are driven by tidal and viscous interactions between the binary and the CBD. We will set up a simplified and idealized model of this picture and see that the phenomena may result in a loss of the binary's orbital angular momentum, a increase in its eccentricity and its faster inspiral.

We thus now assume that a central cavity is surrounded by a CBD. Simulations (references) suggest that in an initially ungapped system the cavity is established after ... binary periods. For simplicity we assume that neither the primary nor the secondary have their own disks. This is also in accordance with Reference, where no inner disks are observed. We aim to relate the viscous angular momentum flux in the inner region of the disk to the orbital evolution of the binary.

The aforementioned numerical simulations (see *e.g.* [5]) suggest that the size of the central cavity extends to about twice the semi-major axis of the binary orbit (as seen from the center of mass frame). This holds for circular orbits. Artymowicz & Lubow [6] showed through simulations that the location of the inner edge progresses outwards with increasing eccentricity, in their simulations

from $r_{in} \approx 1.9a$ for $e \approx 0.02$ to $r_{in} \approx 3a$ for $e \approx 0.6$. These findings are also in accordance with simulations performed by Hayasaki *et al.* [7] where for $e = 0.5$ the inner edge was located at $r_{in} \approx 2.8a$. Also, the above simulations suggest that the gap size seems to be approximately the same for different binary mass ratios q. Inspired by their findings, we thus estimate the inner edge of the circumbinary disk to be set by the twice the distance of the binary at apocenter, *i.e.* $r_{in} = 2a(1 + e)$, and extrapolate this estimate also to eccentricities up to unity. This is not justified and it is likely that modifications occur for higher eccentricities. Towards more definite answers, one has to admit, there is no way around of performing hydrodynamical simulations.

Tidal torques from the binary are expected to act significantly only on a narrow annulus at the inner edge of the CBD and are thus assumed to be zero outside of some cutoff radius r_Λ, which is very similar to r_{in}. Thus the effect of the binary torque on the disk evolution can be accounted for via equation (122) by imposing suitable boundary conditions at the inner edge of the disk. From equation (122) we can thus deduce

$$\left(\frac{\partial(\Omega r^2)}{\partial r} \right) \dot{M} = \frac{\partial(T_{\text{visc}})}{\partial r} + \left(\frac{\partial(\Omega r^2)}{\partial r} \right) \frac{4\pi \Sigma \tilde{T}_{\text{ext}}}{\Omega}. \tag{123}$$

Integrating from r_b to r_Λ we obtain (check this at some point)

$$T_{\text{visc}}(r_\Lambda) = 8\pi \int_{r_b}^{r_\Lambda} dr \, r\Sigma \tilde{T}_{\text{ext}} - 2 \int_{r_b}^{r_\Lambda} dr \, r\Omega \dot{M}; \tag{124}$$

we have set $T_{\text{visc}}(r_b) = 0$ because of the clean gap assumption.

The first integral on the right hand side is the total torque the binary exerts on the disk, that is to say, the rate of the angular momentum injection into the disk by the binary. As long as the evolution of the binary is driven predominantly by the tidal coupling to the disk (and not due to the gravitational wave emission) conservation of angular momentum guarantees that this term equals $-\dot{J}_b$, the change of angular momentum of the binary. In the right integral on the right side we can write

$$\dot{M} = 2\pi \Sigma r v_r = 3\pi \Sigma \nu = 3\pi \Sigma \alpha c_s^2 / \Omega. \tag{125}$$

Because of the clean gap assumption, the disk surface density Σ is zero for $r < r_{in}$. Then we approximate the integral by

$$\begin{aligned}
\Delta &\equiv -6\pi \alpha c_s^2 \Sigma(r_{in}) \int_{r_{in}}^{r_\Lambda} dr \, r \\
&= -3\pi \alpha c_s^2 \Sigma(r_{in}) \left[r_\Lambda^2 - r_{in}^2 \right] \\
&\approx -3\pi \alpha c_s^2 \Sigma(r_{in}) \delta r_{in},
\end{aligned}$$

where we set the disk density in the small radial annulus $[r_{in}, r_\Lambda]$ around the cavity edge to $\Sigma(r_{in})$ since $r_\Lambda - r_{in} = \delta/2 \ll r_{in}$ and since we have no model to resolve the surface density of the CBD down to this scale.

Therefore we may suppose that $T_{\text{visc}}(r_{\text{in}}) = -\dot{J}_b - \Delta$. Recall that we estimate $r_{\text{in}} = 2a(1+e)$, so the viscous torque (117) reads $T_{\text{visc}}(2a) = 12\pi\alpha c_s^2 \Sigma(2a)a^2(1+e)^2$. As this term is a few order of magnitudes higher than Δ, we neglect Δ henceforth.

We impose a further assumption to the particular evolution model, that the binary-disk interaction may well be approximated as an adiabatic process (as opposed to an evolution that is driven by sudden perturbations, like the gravitational wave capture scenario of section 3). That is to say, we assume that the timescale of the disk-binary interaction is much larger than some characteristic timescale of the binary, like its orbital period. It has to emphasized that this is an idealized assumption; it might be supported by the simulations which show the maintenance of the circular shape of the cavity across a large spectrum of eccentricities. Under the adiabatic assumption, the change in the binary energy can be related to its change in angular momentum through the orbital frequency,

$$\dot{E}_b = \Omega_b \dot{J}_b. \tag{126}$$

Note that $\dot{J}_b < 0$, so $\dot{E}_b < 0$ and therefore the binary always evolves toward lower energy. In particular an initially bound orbit always stays on an elliptic orbit. Energy conservation implies that energy is deposited in the circumbinary disk and this dissipated energy may *e.g.* heat up the disk material. From the evolution equation (8) for the semi-major axis of the binary orbit and the binary energy $E_b = -\frac{\Omega_b J_b}{2\sqrt{1-e^2}}$ it follows

$$\frac{\dot{a}}{a} = -\frac{\dot{E}_b}{E_b} = -\frac{T_{\text{visc}}(r_{\text{in}})}{J_b} 2\sqrt{1-e^2} \tag{127}$$

$$= -2\frac{T_{\text{visc}}(r_{\text{in}})}{\mu\Omega_b a^2}, \tag{128}$$

where the last equation follows by substituting the orbital angular momentum (5). Substituting the explicit formula for the viscous torque results in

$$\frac{\dot{a}}{a} = -\frac{24\pi\alpha c_s^2 \Sigma(1+e^2)}{\mu\Omega_b}. \tag{129}$$

Similarly we obtain for the evolution of the eccentricity

$$\frac{e\dot{e}}{1-e^2} = \left(\frac{1}{\sqrt{1-e^2}} - 1\right)\frac{T_{\text{visc}}(r_{\text{in}})}{\mu\Omega_b a^2} \tag{130}$$

$$= \left(\frac{1}{\sqrt{1-e^2}} - 1\right)\frac{12\pi\alpha c_s^2 \Sigma(1+e)^2}{\mu\Omega_b}. \tag{131}$$

We see that while the semi-major axis decreases, the orbital eccentricity increases. Recall that even though we have $\dot{e} > 0$, the orbit cannot become unbound since the orbit's energy decreases.

We use the same values of α, Σ and c_s of the circumbinary disk as those of the background AGN disk. One may argue that these quantities taken at the inner edge of the CBD should not differ significantly from the quantities taken at the outer edge of the CBD and there those quantities should not differ from

their values in the global disk around the central mass M_*. The inspiration for using this assumption comes from Baruteau *et al.* [8], who use exactly the same assumption for the same problem. We use the same assumption due to lack of a better alternative, realizing that likely it is not justified.

4.2.4 Criticism of Model

The implicit assumption on the disk-binary interaction than goes along by employing equation (126) may be formulated in another way. The nonaxisymmetric potential perturbations of the binary are assumed to be small around the average binary potential. This is certainly fulfilled for circular orbits and also for orbits with low eccentricity. For higher eccentricities there is no good reason why this assumption should hold. But since the hydrodynamical simulations do not show signs of a non-circular cavity shapes, we assume the torque to act on average axially-symmetrically onto the disk.

Along the same lines, the use of assumption (126) really reflects our ignorance of the character of the energy flux in the system. For this one needs a microscopic understanding of the disk-binary interaction that does not rely on a macroscopic orbital averaging of dynamical parameters.

In spite of the above dissatisfaction, similar handling is also found in the literature. Hayasaki [9] uses relation (126) and applies it to eccentric orbits up to eccentricity 1. Goldreich & Sari [10] set up a formalism for planet-disk interaction and while explicitly acknowledging that the results are valid only to lowest order in the eccentricity, they apply it eventually to eccentric orbits up to eccentricity 1.

4.2.5 Orbital evolution - Behind the Scenes

UNDER CONSTRUCTION
This section is only valid for low eccentricities. It gives quantitative glimpses of the details of the disk-binary interaction and one might qualitatively use those results to give a deeper understanding of the outlined model of the previous section.

A circular orbit has an angular velocity Omega2 = 1/r dPhi / dr. In linearizing the potential in the neighborhood of a circular orbit, the motion of any particle can be expressed in first order by an epicyclic oscillation, of frequency kappa, Equation 13
The general orbit is therefore the combination of a circle and an epicycle, or a rosette, since there is no rational relation between the two periods.
If the tidal interaction with the binary presents a strong barrier for the gas inflow, then mass accretion onto the binary is vanishingly small. This is the case when the mass ratio is close to unity. For low values of q, tidal torques do not have to completely stop the mass inflow.
In the following we present a model for the migration of the secondary BH which allows to estimate the mass accretion. To this end, we use a (semi-)analytical expression for the tidal torque on the disk from the presence of the secondary mass (in the previous section we ignored the detailed form of the tidal torque).

For a Keplerian disk the surface density evolution (122) is governed by the equation

$$\frac{\partial \Sigma}{\partial t} = \frac{1}{r}\frac{\partial}{\partial r}\left[3r^{1/2}\frac{\partial}{\partial r}\left(\nu\Sigma r^{1/2}\right) - \frac{2r^{3/2}\Sigma\tilde{T}_{\text{tid}}}{M_1^{1/2}}\right], \tag{132}$$

where we incorporated the tidal effect of the disk-secondary interaction through the injection rate of angular momentum per unit mass $\tilde{T}_{\text{tid}}$.

Goldreich and Tremaine in [11] calculated amplitudes of the torque produced by the individual azimuthal Fourier harmonics of the secondary potential. Assumptions: (no restriction to q), and use epicycle approximation (nearly circular orbits). Chandrasekhar page 156 for parametrization. [...] Their result for the radial density torque is

$$\frac{dT}{dr} = \text{sign}(r-a)\frac{\kappa^2 r\Sigma}{2^3 A^4}\frac{M_2^2}{(a-r)^4}\left\{\frac{2\Omega}{\kappa}K_0\left(\frac{\kappa}{2|A|}\right) + K_1\left(\frac{\kappa}{2|A|}\right)\right\}^2. \tag{133}$$

For a Keplerian orbit this simplifies to

$$\frac{dT}{dr} = \text{sign}(r-a)\frac{r\Sigma}{\Omega^2}\frac{M_2^2}{(a-r)^4}\frac{32}{81}\left\{2K_0\left(\frac{2}{3}\right) + K_1\left(\frac{2}{3}\right)\right\}^2 \tag{134}$$

$$\approx \text{sign}(r-a)f\frac{r\Sigma}{\Omega^2}\frac{M_2^2}{(a-r)^4} = \text{sign}(r-a)\Sigma f q^2 M_1\frac{r^4}{(a-r)^4}, \tag{135}$$

with $f \approx 2.5$.

The (unperturbed, not taking epicycle into account) angular momentum of the secondary is $L = M_2 a^2\Omega$. The torque exerted at each ring annulus T_r changes the angular momentum of the secondary according to (angular momentum exchange between the disk and the secondary may cause secular orbital evolution of the secondary)

$$\frac{dL}{dt} = -T_r. \tag{136}$$

Semi-major axis evolution   Thus we find the change in orbital separation due to the torque acting at radius r (using $\kappa(a) = 2\Omega(a)$)

$$\dot{a} = -\frac{2\Omega}{a\kappa^2 M_2}T_r$$

$$= \text{sign}(a-r)\frac{2\pi\Sigma r dr}{2^3\pi A^4}\frac{\Omega M_2}{a(a-r)^4}\left\{\frac{2\Omega}{\kappa}K_0\left(\frac{\kappa}{2|A|}\right) + K_1\left(\frac{\kappa}{2|A|}\right)\right\}^2.$$

For a Keplerian disk this reduces to

$$\frac{\dot{a}}{a} = 0.798\frac{M_2 M_r}{M_1^2}\Omega\left(\frac{a}{a-r}\right)^4\text{sign}(a-r),$$

where $M_r = 2\pi\Sigma r dr$.

Summing all contributions yields

$$\frac{\dot{a}}{a} = 0.798\frac{M_2}{M_1^2}\int_{R_{in}}^{R_{out}} M_r\Omega\left(\frac{a}{a-r}\right)^4\text{sign}(a-r)$$

$$= 2\pi \times 0.798\frac{M_2}{M_1^2}\Omega a^4\left[\int_{R_{in}}^{a'} dr\Sigma\frac{r}{(a-r)^4} - \int_{a''}^{R_{out}} dr\Sigma\frac{r}{(a-r)^4}\right].$$

Tentatively, pulling out Σ and setting $a' = a - \delta$ and $a'' = a + \delta$

$$\frac{\dot{a}}{a} = 2\pi \times 0.798 \frac{M_2}{M_1^2} \Omega a^4 \Sigma \times$$
$$\times \left[\left[\frac{a - 3r}{6(r-a)^3} \right]_{r=R_{in}}^{r=a'} - \left[\frac{a - 3r}{6(r-a)^3} \right]_{r=a''}^{r=R_{out}} \right]. \tag{137}$$

Eccentricity evolution The eccentricity evolution reads

$$\frac{de}{dt} = - \left[(\Omega_p - \Omega) - 2e^2 \Omega \left(1 + \frac{d\log\kappa}{d\log r} \right) \right] \frac{T_r}{M_s e (a\kappa)^2} \tag{138}$$

For the Lindblad resonance we get

$$\frac{\dot{e}}{e} = \frac{\kappa^2 M_2 M_r}{8\pi |A|^5 a |a-r|^5} \left\{ \left[1 + \left(\frac{2\Omega}{\kappa} \right)^2 \right] K_0 \left(\frac{\kappa}{|A|} \right) + \left[\frac{|A|}{\kappa} + \frac{4\Omega}{\kappa} \right] K_1 \left(\frac{\kappa}{|A|} \right) \right\}^2. \tag{139}$$

For the corotation resonances we get

$$\frac{\dot{e}}{e} = - \frac{\kappa^2 M_2 M_r}{8\pi |A|^5 a |a-r|^5} \frac{|A|}{2B} \left\{ \frac{2\Omega}{\kappa} K_0 \left(\frac{\kappa}{2|A|} \right) + K_1 \left(\frac{\kappa}{2|A|} \right) \right\}^2. \tag{140}$$

Evaluating the above equations for Keplerian disks results in

$$\frac{\dot{e}}{e} = 1.523 \frac{M_2 M_r}{M_1^2} \Omega \left(\frac{a}{|a-r|} \right)^5, \tag{141}$$

$$\frac{\dot{e}}{e} = -1.596 \frac{M_2 M_r}{M_1^2} \Omega \left(\frac{a}{|a-r|} \right)^5; \tag{142}$$

the positive term and the negative term come from the Lindblad and the corotation resonances, respectively.

Summing the contributions from successive rings we obtain (here for L-resonances)

$$\frac{\dot{e}}{e} = 2\pi \times 1.523 \frac{M_2}{M_1^2} \Sigma \Omega a^5 \left[\int_{R_{in}}^{a'} dr \frac{r}{|a-r|^5} + \int_{a''}^{R_{out}} dr \frac{r}{|a-r|^5} \right] \tag{143}$$

$$= -2\pi \times 1.523 \frac{M_2}{M_1^2} \Sigma \Omega a^5 \left[\left[\frac{(a-4r)}{12(a-r)^4} \right]_{r=r_{in}}^{r=a'} - \left[\frac{(a-4r)}{12(a-r)^4} \right]_{r=a''}^{r=r_{out}} \right]. \tag{144}$$

4.3 Results from evolution channel

One can combine the evolution equations (129) and (129) of the disk-driven orbital evolution channel with the corresponding gravitational wave driven evolution equations (98) and (99). This coupled system of differential equations can be integrated numerically. Among the various ordinary differential equations solvers in Matlab, the ode23tb function performed best. This solver is designed for solving stiff ordinary differential equations. That the evolution equations exhibit stiffness is as expected, since during the latest stages of inspiral, the solution displays much variation within a short time interval.

As expected, at most values of a the disk-binary interaction dominates the GW emission and this reduces the GW-driven merger time by several orders of magnitudes. The disk-binary dynamics reduces the elliptic binary's semi-major axis while at the same time it increases the elliptic orbit's eccentricity. At a critical semi-major axis, where $\dot{a}_{\mathrm{GW}} = \dot{a}_{\mathrm{disk\text{-}binary}}$, the binary evolution changes from being predominately disk driven to being predominately driven by gravitational wave emission.

Merger Times   Figure (1) shows a comparison between the purely GW-driven merger times (blue) and those where in addition disk interactions are taken into account (green). Here we used $M = 50 M_\odot$; $\mu = M/4$; $a_0 = 10$ AU.
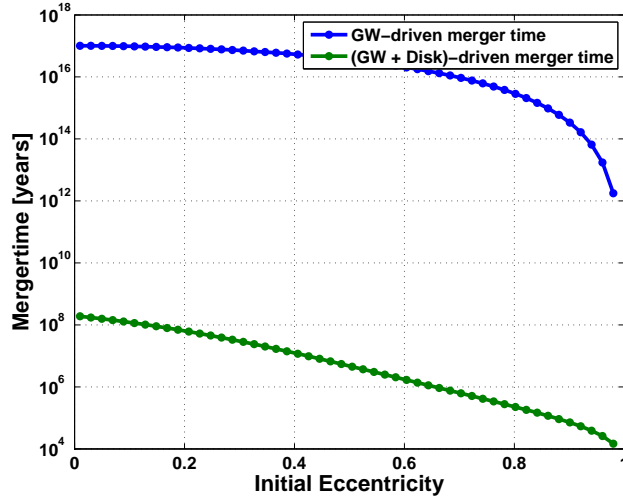

Figure 1: Merger times as a function of the initial binary eccentricity. The blue curve represents the merger times resulting from GW-driven decay, the green one resulting from both GW emission and disk-binary interaction.

In figure (2) the merger times for a binary are plotted as a function of the initial binary semi-major axis a_0 for two different location of the binary in the AGN disk (blue at 0.01 pc, green at 10 pc). As a_0 increases, the merger time decreases.

Eccentricity growth   The eccentricity at the transition semi-major axis (where $\dot{a}_{\mathrm{GW}} = \dot{a}_{\mathrm{disk\text{-}binary}}$) does not necessarily coincide with the maximum eccentricity reached during the orbital evolution. As seen from figure (3), at low eccentricities the eccentricity keeps on growing even after GW has taken over. At higher initial eccentricities the eccentricity approaches unity and then rapidly decays due to GW-emission.
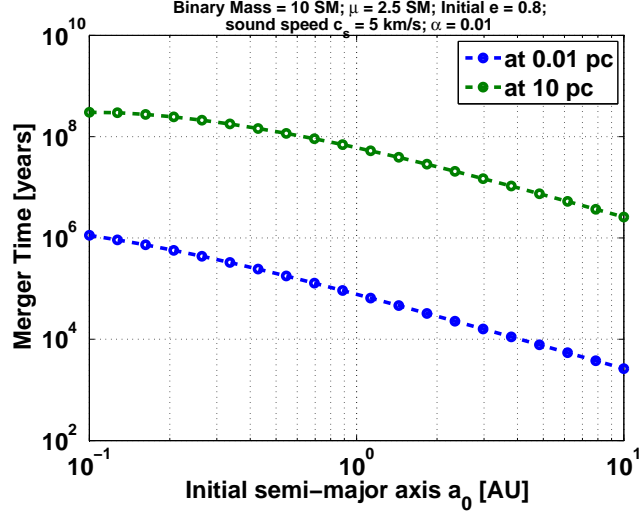
Figure 2: The merger times for a binary as a function of its initial semi-major axis. The two curves stand for two different binary locations in the background disk.
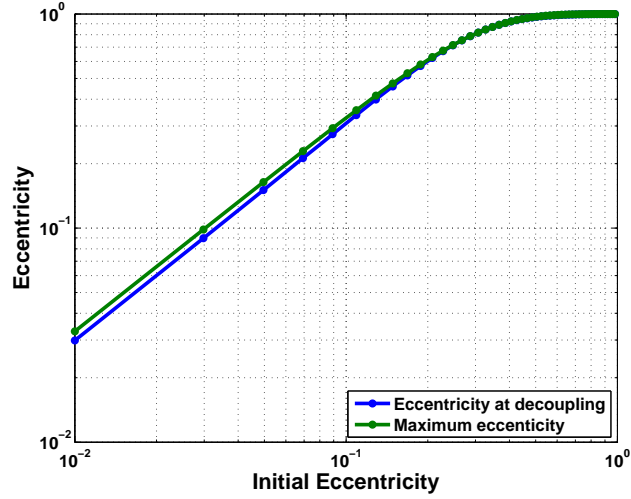

Figure 3: Eccentriicty growth.

5 Merger rate density estimation

In this section we want to estimate the merger rate density that could be expected from the binary evolution channel of the previous chapter. The merger rate density we take as the number of coalescences per unit time per unit volume in the local universe.

We parametrize the rate density of black hole binary mergers in AGN disks in two ways, the second being a refinement of the first. The first parametrization is simply:

$$\mathcal{R}_1 = \frac{N_{\mathrm{BHs}} \, f_b \, n_{\mathrm{AGN}}}{\tau}. \tag{145}$$

Here N_{BHs} is the number of stellar mass black holes per nucleus, f_b is the fraction of black holes residing within binaries (that is, $N_{\mathrm{BHs}} f_b / 2$ is the number of black hole binaries), n_{AGN} is the number density of active galactic nuclei and τ is the average binary merger time. This prescription is similar to the one outlined in McKernan *et al.* [12]. As compared to here, in this paper no attempt is made to estimate the average merger time of binaries, but instead it is assumed that all binaries merge within the lifetime of the disk.

The second prescription for the rate density is more refined and is determined from a weighted average, in the sense described below. Furthermore, the data for $\mathcal{R}_1$ is obtained from an averaging over the data set obtained from the second prescription. Therefore we proceed in setting up the calculation for the latter.

5.1 Mass distributions

We start with an initial stellar distribution. We assume that all stars above a critical mass have evolved into black holes, yielding a BH initial distribution.

Stellar distribution The initial stellar mass distribution seems to follow a multiple power-law function. Here we adopt the initial stellar mass function of Kroupa [13]

$$f_{\mathrm{IMF}}(m) = \begin{cases} k_0 \left(\frac{m}{M_\odot}\right)^{-0.3} & \text{if } m < 0.08 M_\odot \\ k_1 \left(\frac{m}{M_\odot}\right)^{-1.3} & \text{if } 0.08 M_\odot < m < 0.5 M_\odot \, , \\ k_2 \left(\frac{m}{M_\odot}\right)^{-2.3} & \text{if } m > 0.5 M_\odot \end{cases} \tag{146}$$

with normalization parameters $k_0, k_1 = 0.08 k_0$ and $k_2 = 0.04 k_0$. The normalization is taken such that $N_{\mathrm{s,tot}} = \int_{m_{\mathrm{s,min}}}^{m_{\mathrm{s,max}}} dm f_{\mathrm{IMF}}(m)$ and accordingly the parameter k_0 is

$$k_0 = \frac{N_{\mathrm{s,tot}}}{M_\odot} \left/ \left[0.56 - \frac{1}{0.7} \left(\frac{m_{\mathrm{s,min}}}{M_\odot}\right)^{0.7} - \frac{0.04}{1.3} \left(\frac{m_{\mathrm{s,max}}}{M_\odot}\right)^{-1.3} \right]. \right. \tag{147}$$

The total stellar mass is

$$M_* = \int_{m_{\rm s,min}}^{m_{\rm s,max}} dm \, m f_{\rm IMF} \tag{148}$$

$$= k_0 M_\odot^2 \left[0.22 - \frac{1}{1.7} \left(\frac{m_{\rm s,min}}{M_\odot} \right)^{1.7} - \frac{0.04}{0.3} \left(\frac{m_{\rm s,max}}{M_\odot} \right)^{-0.3} \right]. \tag{149}$$

We adopt the "Nuker law" parametrization ([14]) for the stellar density profile $\rho_*(r)$

$$\rho_*(r) \propto \left(\frac{r_b}{r} \right)^\gamma \left[1 + \left(\frac{r}{r_b} \right)^\alpha \right]^{\frac{\gamma - \beta}{\alpha}}, \tag{150}$$

We simplify this profile by using its asymptomatic slopes,

$$\rho_*(r) = \begin{cases} \rho_0 \left(\frac{r}{r_b} \right)^{-\gamma} & \text{if } r \le r_b \\ \rho_0 \left(\frac{r}{r_b} \right)^{-\beta} & \text{if } r > r_b \end{cases} ; \tag{151}$$

the parameter α would parameterize the transition between the inner cusp and the outer power law. The break radius r_b is approximately on the order of the radius of influence of the SMBH ([15]), characterized as $r_b = M_{\rm SMBH}/\sigma_*^2$ (σ_* is the stellar dispersion). The normalization parameter ρ_0 can then be expressed as

$$\rho_0 = \frac{M_*}{4\pi r_b^3} \left(\frac{1}{3 - \gamma} - \frac{1}{3 - \beta} \right)^{-1}, \tag{152}$$

where we used the assumption that we only consider models with $\beta > 3$.

BH distribution   If we assume that every star heavier than $m_{\rm cr}$ evolved into a BH, the total initial number of BHs is

$$N = \int_{m_{\rm s,cr}}^{m_{\rm s,max}} dm \, f_{\rm IMF} \tag{153}$$

$$= k_0 M_\odot \left[0.56 - \frac{1}{0.7} \left(\frac{m_{\rm s,cr}}{M_\odot} \right)^{0.7} - \frac{0.04}{1.3} \left(\frac{m_{\rm s,max}}{M_\odot} \right)^{-1.3} \right] \tag{154}$$

$$= k M_*, \tag{155}$$

where we defined

$$k = \frac{1}{M_\odot} \frac{\left[0.56 - \frac{1}{0.7} \left(\frac{m_{\rm s,cr}}{M_\odot} \right)^{0.7} - \frac{0.04}{1.3} \left(\frac{m_{\rm s,max}}{M_\odot} \right)^{-1.3} \right]}{\left[0.22 - \frac{1}{1.7} \left(\frac{m_{\rm s,min}}{M_\odot} \right)^{1.7} - \frac{0.04}{0.3} \left(\frac{m_{\rm s,max}}{M_\odot} \right)^{-0.3} \right]}. \tag{156}$$

The total mass of all BHs is

$$M_{\rm BH} = \int_{m_{\rm s,cr}}^{m_{\rm s,max}} dm \, m \, f_{\rm IMF}. \tag{157}$$

The BH mass distribution is denoted as $f_{\mathrm{BH}}(m)$ and is normalized such that $\int dm f_{\mathrm{BH}}(m) = 1$. We adopt a Salpeter mass function for the BH distribution

$$f_{\mathrm{BH}}(m) = \xi_0 m^{-2.35}; \tag{158}$$

the normalization parameter ξ_0 is accordingly

$$\xi_0 = -\frac{1.35}{m_{\mathrm{BH,max}}^{-1.35} - m_{\mathrm{BH,min}}^{-1.35}}. \tag{159}$$

If $N(r)$ denotes the total number of BHs inside some radius r, the number dN of BHs lying inside r with masses between m and $m + dm$ is

$$dN = N(r) f_{\mathrm{BH}}(m) dm \tag{160}$$
$$= k M_*(r) f_{\mathrm{BH}}(m) dm, \tag{161}$$

where $M_*(r)$ is the total stellar mass inside radius r $(M_*(\infty) \equiv M_*)$. Note that for the last equality we assumed that the mass distribution of the BHs is independent of the radius at which they reside (an assumption that may not be justified, but still used in the literature). We can write dN in the following form

$$dN = dm\, k\, f_{\mathrm{BH}}(m) \int_0^r dr\, \rho_*(r) 4\pi r^2, \tag{162}$$

and this yields finally

$$\frac{dN}{dm} = \begin{cases} k\, f_{\mathrm{BH}}(m) \frac{4\pi\rho_0}{3-\gamma} r_b^\gamma r^{3-\gamma} & \text{if } r \le r_b \\ k\, f_{\mathrm{BH}}(m) 4\pi\rho_0 r_b^3 \left[\frac{1}{3-\gamma} + \frac{1}{3-\beta} \left[\left(\frac{r}{r_b} \right)^{3-\beta} - 1 \right] \right] & \text{if } r > r_b \end{cases} . \tag{163}$$

The number of BHs with masses between m and $m + dm$ in a radial shell from radius r to $r + dr$ is accordingly

$$\begin{cases} dm\, k\, f_{\mathrm{BH}}(m) \frac{4\pi\rho_0}{3-\gamma} r_b^\gamma \left[(r+dr)^{3-\gamma} - r^{3-\gamma} \right] & \text{if } r \le r_b \\ dm\, k\, f_{\mathrm{BH}}(m) \frac{4\pi\rho_0}{3-\beta} r_b^3 \left[\left(\frac{r+dr}{r_b} \right)^{3-\beta} - \left(\frac{r}{r_b} \right)^{3-\beta} \right] & \text{if } r > r_b \end{cases} . \tag{164}$$

Recall also that the total number of BHs in a radial shell from radius r to $r + dr$ is

$$\begin{cases} k \frac{4\pi\rho_0}{3-\gamma} r_b^\gamma \left[(r+dr)^{3-\gamma} - r^{3-\gamma} \right] & \text{if } r \le r_b \\ k \frac{4\pi\rho_0}{3-\beta} r_b^3 \left[\left(\frac{r+dr}{r_b} \right)^{3-\beta} - \left(\frac{r}{r_b} \right)^{3-\beta} \right] & \text{if } r > r_b \end{cases} . \tag{165}$$

5.2 Rate per galactic nucleus

Now we are in a position to estimate the merger rate per galactic nucleus. To this end we add up the rate contributions coming from different radial shells. We partition the disk into $\mathcal{I}_r$ intervals (we assume that the disk around the SMBH is truncated at 10 pc). The number of BHs within each radial shell $[i\Delta r, (i+1)\Delta r]$, where $\Delta r = 10\mathrm{pc}/|\mathcal{I}_r|$ is obtained from equation (165)

$$N_{r,i} = \begin{cases} k \frac{4\pi\rho_0}{3-\gamma} r_b^\gamma \left[((i+1)\Delta r)^{3-\gamma} - (i\Delta r)^{3-\gamma} \right] & \text{if } (i+1)\Delta r \le r_b \\ k \frac{4\pi\rho_0}{3-\beta} r_b^3 \left[\left(\frac{(i+1)\Delta r}{r_b} \right)^{3-\beta} - \left(\frac{i\Delta r}{r_b} \right)^{3-\beta} \right] & \text{if } i\Delta r > r_b \end{cases} . \tag{166}$$

The average radius within each radial shell is

$$r_i = (i + 0.5)\Delta r. \tag{167}$$

In the rest of this section we assume a binary fraction of unity. This assumption is relaxed later.

5.2.1 Binary BH distributions in a radial shell

In each radial shell, we distribute the BHs according to some canonical binary parameter distribution functions. That is, within each radial shell we assume independent primary mass, mass ratio, orbital separation and eccentricity distributions. The distributions in this subsection refer to a single radial shell $[r, r + dr]$.

Primary mass distribution We adopt the initial mass function of Salpeter for the primary mass distribution. Thus, in a radial shell $[r, r + dr]$, two times the number of binaries with primary mass between m and $m + dm$ is given by equation (164).

Secondary mass distribution The secondary mass distribution is determined by the distribution of the mass ratio q, assumed to follow a uniform distribution (see Tout *et al.* [16] or Ablimit & Maeda [17])

$$f(q) = \mu, \tag{168}$$

where μ is a constant and $0.1 \leq q \leq 1$. The normalization $\mu \int_{0.1}^{1} dq = \frac{1}{2} N_r$ determines μ; N_r is the total number of BHs in the shell $[r, r + dr]$, see equation (166).

Orbital separation distribution The distribution of the initial orbital separation a_0 is assumed to be logarithmically flat (see again [16],[17])

$$f(a_0) = \chi_0/a_0, \tag{169}$$

between the limits 0.01 AU and 500 AU. Normalizations gives $\chi_0 = \frac{N_r}{2 \log 50000}$.

Orbital eccentricity distribution We choose the distribution of the initial orbital eccentricity e_0 to follow a thermal distribution (see [16])

$$f(e_0) = \varsigma_0 e_0, \tag{170}$$

between the limits 0 and 1. Normalization gives $\varsigma_0 = N_r$.

5.2.2 Calculation of rate within a radial shell

We have set up everything to finally perform the calculation of the rate of coalescences in a radial shell. For doing so we partition the various binary distribution functions into discrete intervals and distribute the BHs accordingly among them.

Primary mass   The number of primary BHs within the mass bin $[m_{\text{BH,min}} + i\Delta M, M_{\text{min}} + (i+1)\Delta M]$, where $\Delta M = (m_{\text{BH,max}} - m_{\text{BH,min}})/|\mathcal{I}_M|$ and $i \in \mathcal{I}_M$, is obtained by integrating equation (164)

$$
N_{M,i} = \frac{4\pi k \rho_0 \xi_0}{1.35} \left[(m_{\text{BH,min}} + i\Delta M)^{-1.35} - (m_{\text{BH,min}} + (i+1)\Delta M)^{-1.35} \right] \times
$$
$$
\times \begin{cases} \frac{1}{3-\gamma} r_b^\gamma \left[(r + dr)^{3-\gamma} - r^{3-\gamma} \right] & \text{if } r \leq r_b \\ \frac{1}{3-\beta} r_b^3 \left[\left(\frac{r+dr}{r_b} \right)^{3-\beta} - \left(\frac{r}{r_b} \right)^{3-\beta} \right] & \text{if } r > r_b \end{cases} .
$$

(171)

The average mass within this mass bin is

$$
M_i = \frac{1.35}{0.35} \frac{\left[(m_{\text{BH,min}} + i\Delta M)^{-0.35} - (m_{\text{BH,min}} + (i+1)\Delta M)^{-0.35} \right]}{\left[(m_{\text{BH,min}} + i\Delta M)^{-1.35} - (m_{\text{BH,min}} + (i+1)\Delta M)^{-1.35} \right]} .
$$

(172)

Mass ratio   The number of BBH within the mass ratio bin $[0.1 + i\Delta q, 0.1 + (i+1)\Delta q]$, where $\Delta q = 0.9/|\mathcal{I}_q|$ and $i \in \mathcal{I}_q$, is

$$
N_{q,i} = \frac{10}{18} N_r \Delta q .
$$

(173)

The average mass ratio within this mass ratio bin is

$$
q_i = (i + 0.5)\Delta q + 0.1 .
$$

(174)

Orbital separation   The number of BBH within the orbital separation bin $[0.01\text{AU} + i\Delta a, 0.01\text{AU} + (i+1)\Delta a]$, where $\Delta a = 499.99\text{AU}/|\mathcal{I}_{a_0}|$ and $i \in \mathcal{I}_{a_0}$, is

$$
N_{a_0,i} = \chi_0 \log \left(\frac{0.01\text{AU} + (i+1)\Delta a}{0.01\text{AU} + i\Delta a} \right) .
$$

(175)

The average a_0 within this bin is

$$
a_{0_i} = \frac{\Delta a}{\log \left(\frac{0.01\text{AU} + (i+1)\Delta a}{0.01\text{AU} + i\Delta a} \right)} .
$$

(176)

Orbital eccentricity   The number of BBH within the eccentricity bin $[i\Delta e_0, (i+1)\Delta e_0]$, where $\Delta e_0 = 1/|\mathcal{I}_{e_0}|$ and $i \in \mathcal{I}_{e_0}$, is

$$
N_{e_0,i} = \varsigma_0 (i + 0.5) (\Delta e_0)^2 .
$$

(177)

The average e_0 within this bin is

$$
e_{0_i} = \frac{((i+1)\Delta e_0)^3 - (i\Delta e_0)^3}{3 (i + 0.5) (\Delta e_0)^2} .
$$

(178)

Merger rate for a radial shell The total merger rate resulting from a radial shell is then simply

$$\mathcal{R}_r = N_r \sum_\alpha \frac{N_\alpha}{N_r^4} \frac{1}{\tau_{\mathrm{merger},\alpha}}, \tag{179}$$

where the sum goes over all $\alpha \in \mathcal{I}_M \times \mathcal{I}_q \times \mathcal{I}_{a_0} \times \mathcal{I}_{e_0}$ and $\tau_{\mathrm{merger},\alpha}$ is the time to merger for a binary with parameters α. Note that $N_\alpha = N_{\alpha_1} N_{\alpha_2} N_{\alpha_3} N_{\alpha_4}$.

5.2.3 Merger rate for a galactic nucleus

The galactic merger rate is obtained by summing up the rate (179) for each radial shell,

$$\mathcal{R}_{\mathrm{gal}} = \sum_r \mathcal{R}_r. \tag{180}$$

5.3 Rate density

The merger rate density $\mathcal{R}_2$ is given by

$$\mathcal{R}_2 = \mathcal{R}_{\mathrm{gal}}\, f_b\, n_{\mathrm{AGN}}. \tag{181}$$

The average binary merger time needed for the merger rate density $\mathcal{R}_1$ is obtained by taking the average of all $\tau_{\mathrm{merger},\alpha}$ (see equation (179)).

We adopt the following parameter values, taken from McKernan *et al.* [12]

- $N_{BHs} = 10^3$

- $f_b = 0.7$

- $n_{\mathrm{AGN}} = 2 \times 10^{-5}\ \mathrm{Mpc}^{-3} = 2 \times 10^4\ \mathrm{Gpc}^{-3}$

The remaining parameters we set to

- $M_{\mathrm{SMBH}} = 1 \times 10^6 M_\odot$

- $\gamma = 1.5$

- $\beta = 3.2$

- $\sigma_* = 30\ \mathrm{km/s}$

- $m_{\mathrm{s,max}} = 50000 M_\odot$; $m_{\mathrm{s,min}} = 0.01 M_\odot$; $m_{\mathrm{s,cr}} = 5 M_\odot$

- $m_{\mathrm{BH,max}} = 50 M_\odot$; $m_{\mathrm{BH,min}} = 5 M_\odot$

We use partitions $|\mathcal{I}_r| = 10$ and $|\mathcal{I}_M| = |\mathcal{I}_q| = |\mathcal{I}_{a_0}| = |\mathcal{I}_{e_0}| = 2$. After performing all needed calculations, we obtain the following merger rate densities

- $\mathcal{R}_1 = \frac{10^3 \times 0.7 \times 2 \times 10^4}{2 \times 10^7} \mathrm{year}^{-1}\, \mathrm{Gpc}^{-3} = 0.7\, \mathrm{year}^{-1}\, \mathrm{Gpc}^{-3}$,

- $\mathcal{R}_2 = 5 \times 10^{-4} \times 0.7 \times 2 \times 10^4\, \mathrm{year}^{-1}\, \mathrm{Gpc}^{-3} = 7\, \mathrm{year}^{-1}\, \mathrm{Gpc}^{-3}$.

The rates are not ruled out by LIGO, whose conservative stellar mass BH binary merger rate is $2 - 600\ \mathrm{year}^{-1}\, \mathrm{Gpc}^{-3}$ [18].

To investigate the effect of eccentric orbits on the merger rate, we perform the same calculation as above but set the initial eccentricity to $e_0 = 0.001$ throughout. We obtain $\mathcal{R}_1 = 1 \times 10^{-2}\,\mathrm{year}^{-1}\,\mathrm{Gpc}^{-3}$ and $\mathcal{R}_2 = 2.5 \times 10^{-4}\,\mathrm{year}^{-1}\,\mathrm{Gpc}^{-3}$ respectively. This suggests that ignoring eccentricity changes due to binary-disk interaction underestimates the merger rate. Of course, this conclusion is based on a very simplified and idealised binary merger channel. However, one may still conclude that more detailed studies on the binary-disk interaction will be valuable.

References

1. Thorne, K. S. Multipole expansions of gravitational radiation. *Rev. Mod. Phys.* **52,** 299–339 (2 1980).

2. Watson, G. N. *A Treatise on the Theory of Bessel Functions* (Cambridge University Press, 1966).

3. O'Leary, R. M., Kocsis, B. & Loeb, A. Gravitational waves from scattering of stellar-mass black holes in galactic nuclei. *Monthly Notices of the Royal Astronomical Society* **395,** 2127–2146. ISSN: 0035-8711 (May 2009).

4. Thompson, T. A., Quataert, E. & Murray, N. Radiation Pressure–supported Starburst Disks and Active Galactic Nucleus Fueling. *The Astrophysical Journal* **630,** 167–185 (2005).

5. Lubow, P. S. H. & Artymowicz. *Evolutionary Processes in Binary Stars* (ed R. A. M. J. Wijers, . C. A. T. M. B. Davies) (NATO ASIC Proc. 477, 1996).

6. Artymowicz, P. & Lubow, S. H. Dynamics of binary-disk interaction. 1: Resonances and disk gap sizes. *The Astrophysical Journal* **421,** 651–667 (Feb. 1994).

7. Hayasaki, K., Mineshige, S. & Sudou, H. Binary Black Hole Accretion Flows in Merged Galactic Nuclei. *Publications of the Astronomical Society of Japan* **59,** 427–441. ISSN: 0004-6264 (2007).

8. Baruteau, C., Cuadra, J. & Lin, D. N. C. BINARIES MIGRATING IN A GASEOUS DISK: WHERE ARE THE GALACTIC CENTER BINARIES? *The Astrophysical Journal* **726,** 28 (2010).

9. Hayasaki, K. A new mechanism for massive binary black hole evolution. *Publ. Astron. Soc. Jpn* **61,** 65 (2009).

10. Goldreich, P. & Sari, R. Eccentricity Evolution for Planets in Gaseous Disks. *The Astrophysical Journal* **585,** 1024–1037 (2003).

11. Goldreich, P. & Tremaine, S. Disk-satellite interactions. *The Astrophysical Journal* **241,** 425–441 (Oct. 1980).

12. McKernan, B. *et al.* Constraining Stellar-mass Black Hole Mergers in AGN Disks Detectable with LIGO. *The Astrophysical Journal* **866,** 66 (2018).

13. Kroupa, P. On the variation of the initial mass function. *Monthly Notices of the Royal Astronomical Society* **322,** 231–246 (2001).

14. Lauer, T. R. *et al.* The Centers of Early-Type Galaxies with HST.I.An Observational Survey. *The Astrophysical Journal* **110,** 2622 (Dec. 1995).

15. Schödel, R. *et al.* The distribution of stars around the Milky Way´s central black hole - II. Diffuse light from sub-giants and dwarfs. *A&A* **609,** A27 (2018).

16. Tout, C. A., Hurley, J. R. & Pols, O. R. Evolution of binary stars and the effect of tides on binary populations. *Monthly Notices of the Royal Astronomical Society* **329,** 897–928. ISSN: 0035-8711 (Feb. 2002).

17. Ablimit, I. & Maeda, K. Monte Carlo Population Synthesis on Massive Star Binaries: Astrophysical Implications for Gravitational-wave Sources. *The Astrophysical Journal* **866,** 151 (2018).

18. Abbott, B. P. *et al.* THE RATE OF BINARY BLACK HOLE MERGERS INFERRED FROM ADVANCED LIGO OBSERVATIONS SURROUNDING GW150914. *The Astrophysical Journal* **833,** L1 (2016).

6   Appendix

6.1   Alternative calculation of frequency spectrum

Equation (65) gives the power emitted in the n-th harmonic of an elliptic Keplerian orbit. Here there is similar derivation of the same result which does not explicitly use Parseval's identity. Again, we parametrize an elliptic Keplerian orbit in the following form

$$x(\beta) = a(\cos u - e), \tag{182}$$
$$y(\beta) = b\sin u. \tag{183}$$

Here a is the semi-major axis and b is the semi-minor axis of the orbit. The eccentric anomaly u is defined by the Kepler equation

$$u - e\sin u = \omega(t - t_0) \equiv \beta, \tag{184}$$

the time t_0 being an integration constant chosen such that $x(-\beta) = x(\beta)$ and $y(\beta) = -y(-\beta)$. The solution of the Kepler equation can be given as a Fourier expansion involving Bessel functions. To see this we make the Fourier series ansatz

$$y(\beta)\frac{e}{b} = u - \beta = e\sin u = \sum_{n=1}^{\infty} a_n \sin(n\beta), \tag{185}$$

where the coefficients are given by

$$a_m = \frac{2}{\pi}\int_0^{\pi} d\beta\,(u - \beta)\sin(m\beta). \tag{186}$$

We now compute

$$\begin{aligned}
a_m &= -\frac{2e}{\pi m}\int_0^{\pi} d\beta\,\sin u\,\frac{d}{d\beta}\cos(m\beta)\\
&= \frac{2e}{\pi m}\int_0^{\pi} du\,\frac{d\sin u}{du}\,\cos(m\beta)\\
&= \frac{2e}{\pi m}\int_0^{\pi} du\,\cos u\,\cos(mu - me\sin u)\\
&= \frac{e}{m}\int_0^{\pi}\frac{du}{\pi}\,\left[\cos(u(m-1) - me\sin u) + \cos(u(m+1) - me\sin u)\right].
\end{aligned}$$

By using the following integral representation of the Bessel functions of the first kind

$$J_n(z) = \int_0^{\pi}\frac{du}{\pi}\cos(nu - z\sin u), \tag{187}$$

we arrive at

$$a_m = \frac{e}{m}\left[J_{m-1}(me) + J_{m+1}(me)\right]. \tag{188}$$

Using the recurrence formula

$$J_{n-1}(z) + J_{n+1}(z) = \frac{2n}{z}J_n(z), \tag{189}$$

this result can be rewritten as

$$a_m = \frac{2}{m} J_m(me). \tag{190}$$

Similarly we write $\frac{x(\beta)}{a} = \cos u - e = b_0 + \sum_{n=1}^{\infty} b_n \cos(n\beta)$ and find for the corresponding expansion coefficients

$$b_0 = -\frac{3}{2}e, \tag{191}$$

$$b_m = \frac{1}{m}[J_{m-1}(z) - J_{m+1}(z)] = \frac{2}{m} J_m'(me); \tag{192}$$

the prime denotes the derivative with respect to the argument. Next we compute the Fourier expansion of $x^2(\beta)$, $y^2(\beta)$ and $x(\beta)y(\beta)$. We can again write

$$y^2(\beta) = A_0 + \sum_{n=1}^{\infty} A_n \cos(n\beta), \tag{193}$$

$$x^2(\beta) = B_0 + \sum_{n=1}^{\infty} B_n \cos(n\beta), \tag{194}$$

$$y(\beta)x(\beta) = \sum_{n=1}^{\infty} C_n \sin(n\beta), \tag{195}$$

together with

$$A_m = \frac{2}{\pi} \int_0^{\pi} d\beta \, y^2(\beta) \cos(m\beta), \tag{196}$$

$$B_m = \frac{2}{\pi} \int_0^{\pi} d\beta \, x^2(\beta) \cos(m\beta), \tag{197}$$

$$C_m = \frac{2}{\pi} \int_0^{\pi} d\beta \, x(\beta)y(\beta) \sin(m\beta). \tag{198}$$

Similar to the calculation of a_n we obtain

$$A_m = \frac{b^2}{m} \left[J_{m+2}(me) - J_{m-2}(me) \right],$$

$$B_m = \frac{a^2}{m} \left[J_{m-2}(me) - J_{m+2}(me) - 2e(J_{m-1}(me) - J_{m+1}(me)) \right],$$

$$C_m = \frac{ba}{m} \left[J_{m+2}(me) + J_{m-2}(me) - e(J_{m+1}(me) + J_{m-1}(me)) \right],$$

along with $A_0 = \frac{1}{2}$ and $B_0 = \frac{1+4e^2}{2}$. By the use of the recurrence relations (189) and (192) the above relations can be expressed entirely in terms of J_m and its derivative. We obtain

$$A_m = \frac{4b^2}{me} \left[\frac{1}{me} J_m(me) - J_m'(me) \right],$$

$$B_m = \frac{4a^2}{m} \left[\left(\frac{1}{e} - e \right) J_m'(me) - \frac{1}{me^2} J_m(me) \right], \tag{199}$$

$$C_m = \frac{4ba}{m} \left[\left(\frac{1}{e^2} - 1 \right) J_m(me) - \frac{1}{me} J_m'(me) \right].$$

With the above we are able to expand the second mass moment (18) as

$$\mathcal{G}_{a_1 a_2} = \mu \sum_{n=0}^{\infty} \begin{bmatrix} B_n \cos(n\beta) & C_n \sin(n\beta) & 0 \\ C_n \sin(n\beta) & A_n \cos(n\beta) & 0 \\ 0 & 0 & 0 \end{bmatrix}_{a_1 a_2} \equiv \sum_{n=0}^{\infty} \mathcal{G}_{a_1 a_2}^{(n)}. \qquad (200)$$

The emitted power in the quadrupole approximation is obtained from the formulae (13) and (26)

$$P = \frac{8\pi}{75} \sum_{m=-2}^{2} \left\langle \left| {}^{(3)}\mathcal{G}_{a_1 a_2} \left(\mathcal{Y}_{a_1 a_2}^{2m} \right)^* \right|^2 \right\rangle. \qquad (201)$$

Since $\langle \cos(n\beta) \cos(m\beta) \rangle = \langle \sin(n\beta) \sin(m\beta) \rangle = \frac{1}{2}\delta_{mn}$, different harmonics don't contribute in the power spectrum. Hence we can set $P = \sum_{n=1}^{\infty} P_n$, where the power radiated in the n-th harmonics is

$$P_n = \frac{8\pi}{75} \sum_{m=-2}^{2} \left\langle \left| {}^{(3)}\mathcal{G}_{a_1 a_2}^{(n)} \left(\mathcal{Y}_{a_1 a_2}^{2m} \right)^* \right|^2 \right\rangle, \qquad (202)$$

together with

$$ {}^{(3)}\mathcal{G}_{a_1 a_2}^{(n)} = \mu(\omega n)^3 \begin{bmatrix} B_n \sin(n\beta) & -C_n \cos(n\beta) & 0 \\ -C_n \cos(n\beta) & A_n \sin(n\beta) & 0 \\ 0 & 0 & 0 \end{bmatrix}_{a_1 a_2}. \qquad (203)$$

Using the above formulae gives the power in the n-th harmonic as

$$P_n = \frac{1}{15} \mu^2 (\omega n)^6 \left(A_n^2 + B_n^2 + 3C_n^2 - A_n B_n \right). \qquad (204)$$

We can now insert the explicit form of the coefficients (199) and after rearranging terms we find that P_n is equal to (65).